

Room-Temperature Silicon Carbide Maser: Unveiling Quantum Amplification and Cooling

Andreas Gottscholl^{1,2,a)}, Maximilian Wagenhöfer¹, Valentin Baianov¹, Vladimir Dyakonov¹,
Andreas Sperlich^{1,b)}

¹Experimental Physics 6 and Würzburg-Dresden Cluster of Excellence ct.qmat,
Julius-Maximilians-Universität Würzburg, 97074 Würzburg, Germany

²NASA Jet Propulsion Laboratory, California Institute of Technology, Pasadena, California,
USA

a) Electronic mail: andreas.p.gottscholl@jpl.nasa.gov

b) Electronic mail: andreas.sperlich@uni-wuerzburg.de

Abstract

We present the very first demonstration of a maser utilizing silicon vacancies (V_{Si}) within 4H silicon carbide (SiC). Leveraging an innovative feedback-loop technique, we elevate the resonator's quality factor, enabling maser operation even above room temperature. The SiC maser's broad linewidth showcases its potential as an exceptional preamplifier, displaying measured gain surpassing 10dB and simulations indicating potential amplification exceeding 30dB. By exploiting the relatively small zero-field splitting (ZFS) of V_{Si} in SiC, the amplifier can be switched into an optically-pumped microwave photon absorber, reducing the resonator's mode temperature by 35 K below operating conditions. This breakthrough holds promise for quantum computing advancements and fundamental studies in cavity quantum electrodynamics. Our findings highlight SiC's transformative potential in revolutionizing contemporary microwave technologies.

Introduction

Lasers have become an indispensable part of our everyday lives. From high-power lasers in manufacturing technology to high-precision lasers in metrology or monochromatic light sources for research, lasers and their enormous applicable potential is ubiquitous [Kawahito et al. 2018, Udem et al. 2022]. The fundamental process of stimulated emission based on a population inversion is however older than the laser and was previously investigated for microwave photons instead of optical ones [Lamb et al. 1964, Gordon et al. 1955] which is also known as a maser (microwave amplification of stimulated emission).

A broad application of a maser, however, is currently not predictable. So far masers were only used as low-noise amplifier and clock-standards depending on their linewidth and stability. This is owed to the very unfavorable operating conditions such as vacuum techniques for free-electron and atomic masers and cryogenic temperatures for solid state masers [Konoplev, et al. 2006, Kleppner, et al. 1962, Siegman et al. 1964]. Therefore, the enormous (and so far unpredictable) potential of masers has not yet been exploited.

Despite these challenges, recent advancements in spin-defect masers and other approaches, such as the exploitation of Floquet systems [Jiang et al. 2021], have opened new possibilities for overcoming these limitations. Among spin-defect masers, which promise fast and versatile application due to their comparatively simple design, there are

two known systems so far [Rodriguez et al. 2023]: On the one hand Oxborrow et al presented the first room temperature maser using organic materials (e.g. pentacene-based) with a pulsed maser output at 1.45 GHz, which is currently developed towards a continuous wave (CW) output [Oxborrow et al. 2012, Breeze et al. 2015, Breeze et al. 2017, Wu et al. 2020, Ng et al. 2023]. On the other hand, room temperature masers were demonstrated with NV⁻ centers in diamond providing enhanced thermal and mechanical properties [Breeze et al. 2018, Zollitsch et al. 2023, Wu Q et al. 2023]. Due to its EPR-based (electron paramagnetic resonance) principle it operates at a X-band frequency of 9.2 GHz in a CW mode. In general, its frequency can be tuned to an arbitrary frequency by the external magnetic field and is only limited to the resonance frequency of the used resonator. Besides the existing maser systems, another promising candidate are silicon vacancies in 4H silicon carbide (SiC) [Arroo et al. 2021, Kraus et al. 2014, Gottscholl et al. 2022]. Their very small ZFS of only $2D/h = 70$ MHz makes the SiC maser attractive for applications within the entire communication band, since a small ZFS corresponds to a very broad frequency tunability, since population inversion of the maser transition is reached already for small bias magnetic fields. However, a fully operating maser has been illusive so far. SiC is known as a well-established semi-conductor material in industry and can be fabricated on wafer-scale. Thus, a maser based on this standard material would make the new generation of spin-defect masers – besides an exciting platform for cavity quantum dynamics – to a gamechanger in our everyday life microwave applications with the potential of revolutionizing state-of-the-art preamplifiers and coherent microwave sources [Rodriguez et al. 2023].

In this work we present for the very first time a SiC-based maser. We are analyzing the linewidth and output patterns regarding output frequency and swept external magnetic field. The simplest configuration with SiC in a resonator and optically pumped by a laser reveals a low output power at $T = 110$ K. To address critical parameters and enhance output power, we study key influences, including the optical pumping of the gain medium and the quality (Q-factor) of the resonator. The latter is achieved by the implementation of a feed-back loop which enables an artificial enhancement of the effective Q-factor. Together with a theoretical model solving the Langevin equations (see [Jin et al. 2015] for details) we can estimate the potential of a SiC-based maser. Addressing these issues, we demonstrate masing exceeding room temperature operation at 315 K (due to laser heating). Moreover, we present a SiC-based low noise amplifier by inserting an external microwave signal into our device. Furthermore, by shifting the magnetic field up by 5 mT to address the de-populated spin transition, we invert the amplification effect and we can use our system as an optically-pumped microwave photon absorber. With this effect we are able to demonstrate a microwave refrigerator by reducing the mode temperature of the used microwave frequencies by 35 K. Finally, we compare the properties of SiC with those of other maser systems and highlight the large potential of these results for quantum computing based on superconducting qubits.

Silicon Carbide as gain medium

The basic principle of a maser is identical to a conventional laser and is illustrated in Figure 1a [Oxborrow et al. 2012, Breeze et al. 2018]. The maser consists of three major parts: 1) a gain material, 2) an optical pumping in order to achieve a non-equilibrium condition (population inversion) and 3) a resonator in which the gain material is placed which enhances the interaction of microwaves and gain material. In the following we want to discuss the different components.

1) Gain material based on SiC: For the gain material we choose a wide-spread material which can hosts spin defects with energy levels that enable transitions in the microwave photon energy regime. Since SiC can host a variety of different spin defects which reveal an electron paramagnetic resonance (EPR) signature, these defects are perfect candidates for a potential maser. One of the most investigated spin defects is the silicon vacancy V₂ in the polytype 4H SiC. Especially, the spin polarization of this system under optical excitation is substantial for a gain medium. The pumping scheme is shown in Figure 1b. The system possesses a quartet ground spin state ($S=3/2$), which can be optically excited by photons in the near infrared [Orlinski et al. 2003, Kraus et al. 2014].

2) Optical pumping: Since the excited state relaxes spin-dependent, we end in a spin polarization of the ground state. Similar to a laser, a maser also requires a population inversion. To achieve this inverted population difference, we apply an external magnetic field of $\gg 2.5$ mT (corresponding to 70 MHz). This overcomes the ground state level anti-crossing (GSLA), where the energy levels are differently distributed due to the Zeeman effect [Anisimov et al. 2016]. If now an incoming microwave photon possesses the same energy as the Zeeman-split transition energy, it leads to an avalanche of coherent microwave photons [Breeze et al. 2018]. The incoming photon can be part of a signal if the maser is used as a low noise amplifier, or it can start due to spontaneous emission which leads to a maser as a coherent microwave source. To achieve a sufficient coupling of the microwaves to the spin system, a resonator with a high quality is required.

3) High-Q resonator: The resonator for the here-reported SiC maser consists of two parts: a cylindrical metallic copper resonator and a dielectric sapphire core in the center which contains the SiC gain material. The sapphire ring concentrates the microwaves in the center, reducing the ohmic losses in the copper wall and leading to a higher Q-factor, which is the figure of merit for the resonator's quality. The magnetic field components of the microwaves are illustrated in purple in Figure 1a. A coupling antenna outcouples the created microwaves into a standard SMA cable to enable characterization of the microwave output and finally use the maser as a coherent microwave source. A detailed analysis of the resonator is given in the SI.

SiC-based maser

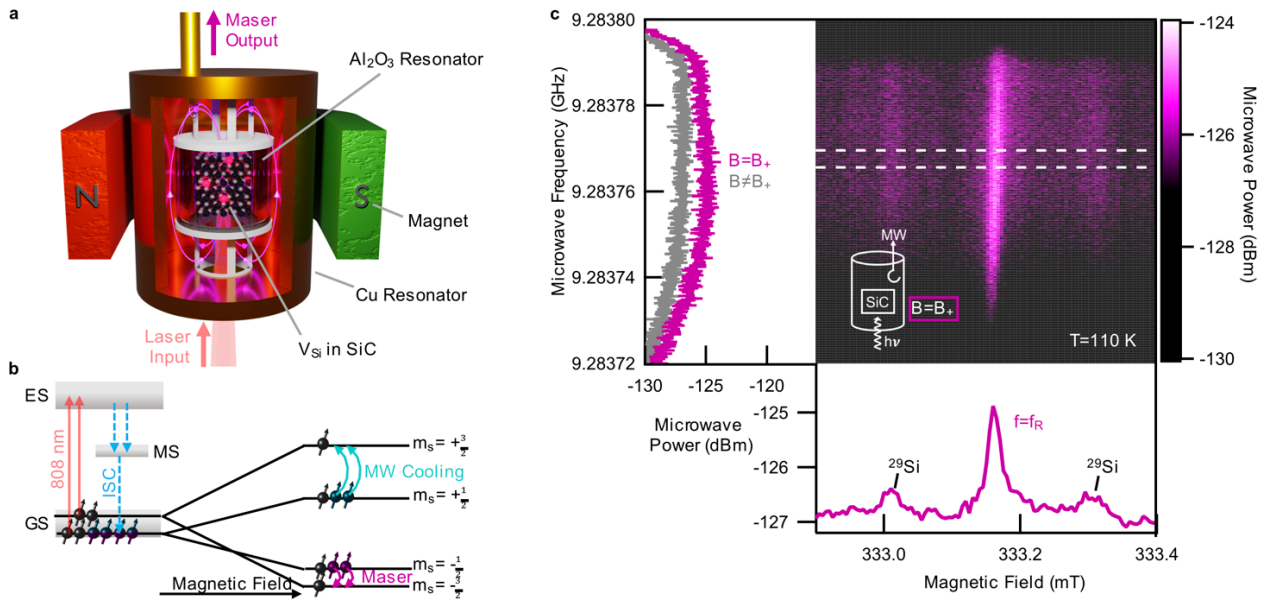


Figure 1: Silicon carbide-based maser: **a** Basic principle: maser output is achieved by optical pumping of the gain material (SiC) in a high-Q resonator inside an external magnetic field. **b** Pumping scheme of the gain material: a population inversion is created by an external magnetic field which can be used for the maser process (pink). The second spin polarized transition (blue) can be used for a microwave refrigerator. **c** Maser output measurement while sweeping the magnetic field at $T=110$ K: the color map reveals a broad emission peak displayed in the frequency domain (left plot) and over the magnetic field (bottom plot). The microwave power plotted vs. the magnetic field is the average maser output power in between the two dashed lines. A narrow peak is observed at the resonant transition $B=B_+$ with two satellite peaks according to hyperfine interaction with ^{29}Si isotopes. The inset illustrates the setup configuration, a detailed description can be found in Figure S4 of the SI.

In order to demonstrate a SiC-based maser, microwave amplifier and refrigerator in this work, the standard measurement method is the detection of the microwave intensity in a specific frequency band with a spectrum analyzer attached to the end of the SMA cable of the coupling antenna (see Figure S1 for detailed setup description). The external magnetic field is tuned by using magnetic field coils within the range of the expected emissive/absorptive transition. In principle an arbitrary magnetic field can be used above the ground state level anti-crossing (GSLA). However, the corresponding frequency has to fit to the resonance frequency of the resonator which is in the case 9.3 GHz corresponding to a resonant magnetic field of about $B_+ \approx 333$ mT. The resonator is incorporated in a cryostat to perform measurements at lower temperatures ($T=110$ K). In this environment the population inversion is easier to achieve due to the longer spin-lattice relaxation times [Simin et al. 2017]. Furthermore, the Q-factor is higher since the ohmic losses are reduced in the cooper walls. The noise level due to thermal microwave photons is around -130dBm. Figure 1c shows the frequency resolved output power of this configuration for a swept magnetic field around the resonant condition ($B_+=333.19$ mT) and a sufficient high pump power ($P_{\text{Laser}}=450$ mW) of an 808 nm excitation. The intensity of the color map represents the microwave output power which reveals a pattern with three narrow features: one pronounced signal in the center and two outer peaks. To study it more in detail the bottom figure reveals the average

maser power within the two dashed white lines. We can now clearly extract a narrow peak with a linewidth of 0.021 mT (corresponding to 588 kHz) and a total amplitude of -125dBm (corresponding to ~300 aW). This small signal is attributed to the silicon vacancy since it arises at the correct magnetic field and shows two additional satellite peaks. These are related to the ^{29}Si isotopes surrounding the silicon vacancies with a natural abundance of 4.7%, leading to a shifted resonance condition due to hyperfine splitting (150 μT). With this measurement, we demonstrate the first SiC-based maser in a CW mode. However, as we can see for the slice in the frequency domain (left subfigure of Figure 1c) the signal rises just marginally from the thermal background. In order to enhance the output power and realize room temperature masing, we address critical parameters such as optical pumping and the Q-factor of the resonator.

Q-boosted maser

In general, the generation of microwave photons $|a|^2$ can be quantified by solving the Langevin equations as described elsewhere [Jin et al. 2015] which leads to:

$$|a|^2 = \frac{\omega - \gamma_{\text{eg}}}{2\frac{\omega_c}{Q}} N - \frac{\omega + \gamma_{\text{eg}}}{2\frac{\omega_c}{Q}} S_z \quad [1]$$

Here, the pump rate ω is given by the effective optical pump power $P_{\text{Laser}} = \omega \frac{hc}{\lambda}$, $\gamma_{\text{eg}} = T_1^{-1}$ is the spin lattice relaxation rate, ω_c and Q are the frequency and quality factor of the resonator, respectively. N is the number of participating spins and $S_z = \frac{\kappa_S \kappa_C}{4g^2}$ the number of polarized spins mainly given by the coupling constant g and the collective decay rate $\kappa_S \approx \frac{2}{T_2^*}$ limited by the coherence time T_2^* . In order to realize a working maser, a microwave output is required, thus $|a|^2 > 0$ defines the maser threshold. Inserted into equation [1] the following expression can be derived as limit for the necessary Q-factor:

$$Q \geq \frac{\omega + \gamma_{\text{eg}}}{\omega - \gamma_{\text{eg}}} \frac{\kappa_S \omega_c}{4Ng^2} \quad [2]$$

In Figure 2a, we show the expected microwave power according to equation [1] for our SiC maser for a broad range of different Q-factors and optical pump powers. Two thresholds are relevant: the pump threshold $\omega > \gamma_{\text{eg}}$ (vertical grey dashed line) and the maser threshold according to equation [2] (black dashed curve). The pump threshold is mainly given by the T_1 time and can be exceeded by increasing the pump power. The maser threshold, however, strongly depends on the coupling and the coherence time T_2^* of the system and can be reached by increasing the quality factor of the resonator.

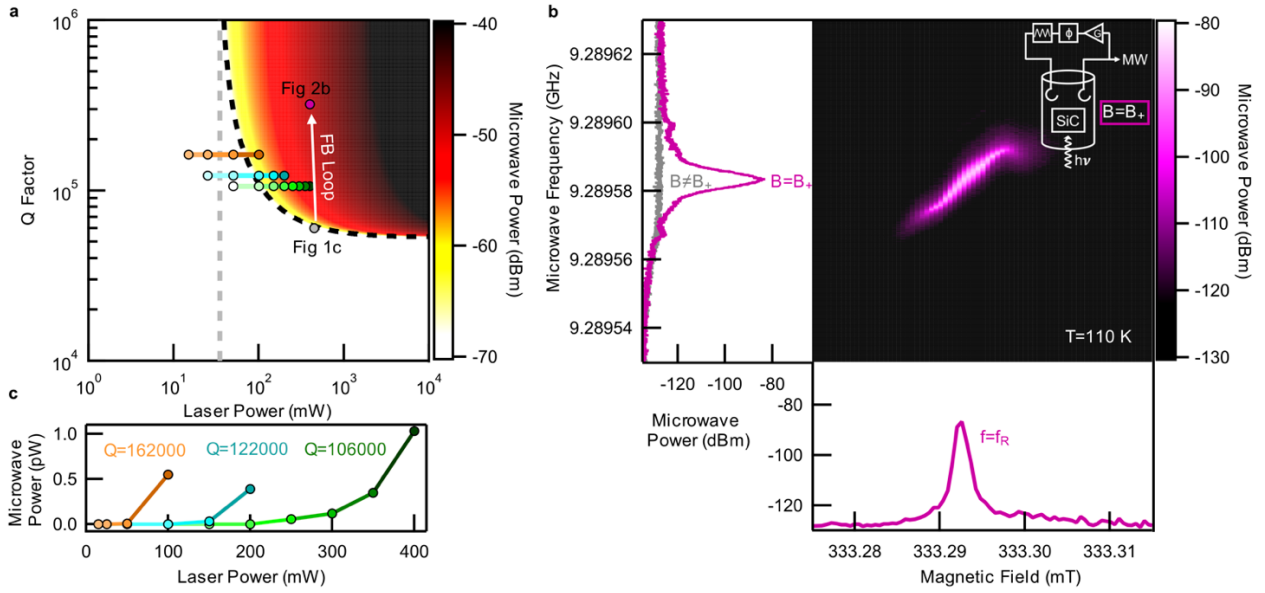


Figure 2: Q-booster maser at 110 K. **a** Theoretical model of a SiC-based maser: the masing regime is indicated by the black dashed line while the grey dashed curve shows the pump threshold for achieving a population inversion. **B** Maser output of a feedback-loop (FB) driven maser at 110 K: the left sub-plot displays a sharp peak in the frequency domain while the bottom graph shows the in-resonance cross-section over the magnetic field. The inset illustrates the setup configuration, a detailed description can be found in Figure S5. **c** The observed maximum maser output for a large range of optical pumping power and Q-factors. All measurements are inserted in the theoretical model (a).

With the used parameter set (see SI for more details) we explain the very low maser power of Figure 1c by a maser being directly at the maser threshold. The measurement of Figure 1c and also the following measurements are inserted as points into the simulation. We now aim to enhance the SiC maser by further entering the masing regime. This improvement can be achieved either by increasing the coherence time or by changing the resonator properties. The first can be realized by isotopical purification of ^{28}SiC [Simin et al. 2016, Lekavicius et al. 2022] but is not in the scope of this work. A more continuous method of studying the maser involves changing the quality of the resonator in use. A very powerful tool is the implementation of a feedback-loop enabling an artificial enhancement of the Q-factor (see Figure S5 for details) [Lesage et al. 1981, Wu H et al. 2023]. In general, the Q-factor is defined by the energy losses per cycle. However, if the resonator is feed with its own microwave output, the energy losses can be reduced and the Q-factor is enhanced artificially. This is achieved by an outcoupling of the microwaves with the same antenna as in the previous measurement, but half of the signal (-3dB) is amplified and inserted phase-corrected back into the resonator. Now, we are able to boost the Q-factor of measurement Figure 1c by a factor of 5 which is illustrated in Figure 2a (grey and purple circles).

The feedback-loop driven maser measurement of the frequency resolved output power versus the swept magnetic field is depicted in Figure 2b. We choose a narrower magnetic field range in order to study the shape of the microwave peak in magnetic field direction. The color map reveals an S-shape pattern which is due to the overlap of the Lorentzian peak contribution in f -direction and a Lorentzian peak in B -direction due to the natural line width of the EPR transition [Breeze et al. 2018]. The output power is reaching to almost -80dBm (several fW) making it already usable for practical applications. A cross section through the

center of the S-shape is depicted in the bottom sub-plot of Figure 2b. The linewidth 0.001mT of the microwave output is much narrower than in the previous measurement of Figure 1c (factor of 21). We performed several feedback-loop driven maser measurements (see Figure S14) to study the influence of Q-factor and microwave power which are depicted in Figure 2c. We can observe that the maser output strongly depends on the Q-factor which coincides with the simulation. For higher Q-factors, a lower laser power is required to reach the maser threshold. The measured values are also inserted into the simulated masing regime. However, the output power is still lower than the expected ideal output power of the simulation which is mainly owed to coupling losses of the antenna but also losses between the many connectors of the SMA components of the setup (see SI for signal discussion of the setup). Nevertheless, we can present a drastic improvement of the signal quality and strength by an artificial enhancement of the Q-factor which reveals the large potential of this SiC-based maser.

SiC-based maser at room temperature

The so far presented results were all performed at cryogenic temperatures ($T=110$ K). To enable masing even above room temperature, we use the Q-boosted approach to lower the maser threshold. In Figure 3 a maser output measurement at 315 K is presented. The temperature is slightly above room temperature since a sufficient high optical pump power of 617 mW is required to overcome the maser threshold. At this temperature, the resonance condition occurs at lower magnetic fields due to the lower resonance frequency of the thermally expanding resonator dimensions (see Figure S10 for temperature dependence). The observed signal contains two features: first, a very intense microwave output at the resonant conditions ($f=f_R$ and $B=B_+$) and second, a continuous trace with variable frequency. The first signal (the actual maser output) reveals a very high microwave output of -40dBm. This is related to the very sensitive feedback loop which has to be set to a high amplifying mode in order to reach the maser threshold at room temperature. This amplification mode is visible in a cross-section, as depicted in the bottom sub-plot of Figure 3. A massive increasing of the broadening can be observed in comparison to the previous measurements. The reason is, that the signal is already reaching the maser regime with the Q-boosted resonator for magnetic fields at the edges of the magnetic resonance condition. The maser output with frequency resolution, however, is narrower as displayed on the left of Figure 3. This linewidth can be considered as the actual linewidth of the maser, representing the frequency domain used in practical applications. The broad plateau with its linewidth of 0.04 mT is in fact a large advantage since it demonstrates the stability of the maser over magnetic field fluctuations. If this peak would be narrower, the maser output would collapse for a small magnetic field deviation which limits the application of the proposed maser device. The most critical component we observed is the stability of the resonator frequency of our device. If the frequency shifts due to temperature fluctuations/drifts, the whole maser frequency is shifting accordingly. This resonance frequency change can be observed when analyzing the continuous trace since this signal contribution is related to thermal photons within the resonator, which are amplified by the very sensitive feedback loop. These can be used for tracking the resonance frequency without performing Q-factor measurements. Therefore, the random trace directly provides insights into the resonance frequency shift of our systems and highlights this most critical aspect for a stable maser device. For future applications, the resonance frequency has to be stabilized/controlled to get a reliable maser output frequency.

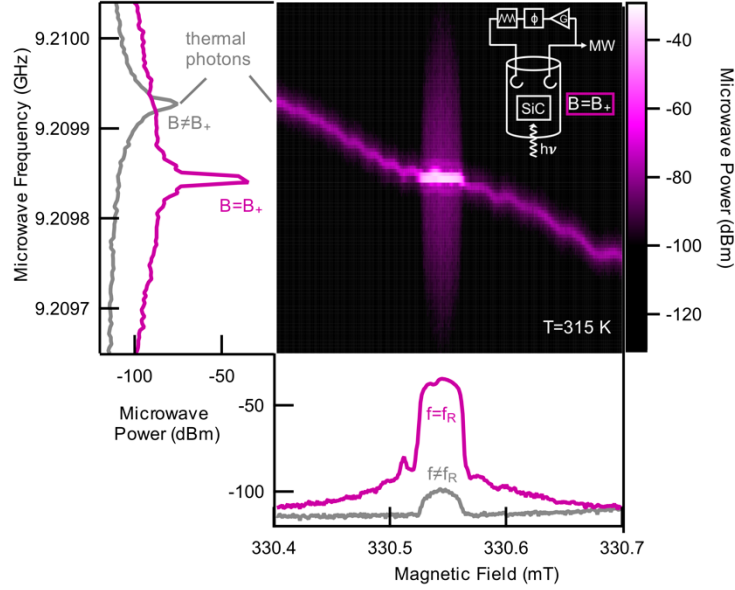


Fig.3: Q-boosted maser at $T=315$ K: The color map reveals a high output power of -40 dBm (white region) at $f=f_R$ and $B=B_+$. The purple trace is given by the amplified thermal photons inside the cavity (see text for details). A cross section at a non-resonant magnetic field $B \neq B_+$ (grey) shows an enhancement effect of thermal microwave photons.

To conclude, a SiC-based maser has been realized. At low temperatures the maser threshold can be directly reached, and stable maser operation has been observed with a very narrow signal output. Using a feedback loop, the Q-factor is artificially enhanced, enabling masing even above room temperature. However, so far, this yields a relatively broad signal due to the used feedback loop. Therefore, the use as a signal amplifier would be intriguing. Especially for frequency-modulated signals, which are often the basis of our everyday communication protocols, a broader frequency range is preferred, thus making the presented SiC maser an ideal candidate for low-noise preamplifiers. In the following, we address and investigate the capability of our system for amplifier applications.

SiC-based amplifier

Besides the application of a maser as a coherent microwave source, the SiC maser can be used as a low noise amplifier of weak microwave signals. The configuration is identical to the setup of the feedback-loop, with the exception that an external signal is fed into the resonator instead of its own microwave output (see inset in Figure 4 and Figure S4 for details). We analyzed this behavior by inserting weak microwave signals with one antenna and measuring the output by the second antenna while sweeping the magnetic field. The result is depicted in Figure 4a. The horizontal line is the inserted constant microwave signal (which is within the linewidth of the resonator). While sweeping the magnetic field, we can observe an amplification of the signal at the resonant magnetic field. A cross section is shown in the bottom sub-plot of Figure 4a. We choose the magnetic field sweep broad enough to also study the influence of the ^{29}Si hyperfine peaks. The optically-pumped gain medium amplifies the signal by 7dB (1.8dB for hyperfine peaks) which makes it ideal for a low-noise preamplifier. No broadening of the signal can be observed, as depicted in the left sub-plot of Figure 4a ($B = B_+$: amplifier on, $B \neq B_+$: amplifier off). To reveal the full potential

of this preamplifier, we simulated the gain for different Q-factors and different pump powers which is shown in Figure 4b. In principle, the amplifier can amplify weak signals by several orders of magnitude. This theoretical model is verified by further measurements with varied Q-factors (shown in blue) and variable pump power (shown in green). The corresponding measurements are displayed in Figure 4c. The amplification can be enhanced by increasing the Q-factor as well as by increasing the optical pump power. Thus, we observe the highest amplification of the signal by 11dB for a laser power of 500 mW. In general, we can also observe and simulate that the amplification is higher for weaker signals which is shown with the orange circles in Figure 4c (see Figure S13 for corresponding simulations).

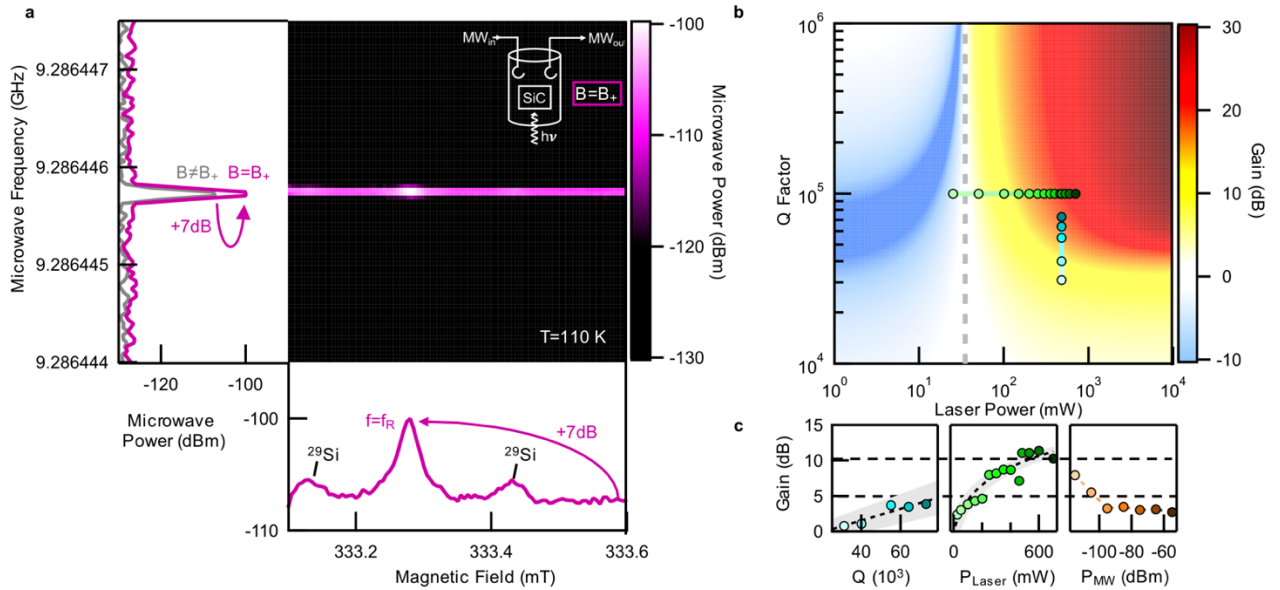


Fig.4: SiC-based amplifier using the maser transition at T=110 K. **a** Color map of the measured microwaves: a narrow purple line is given by the inserted microwave signal. As soon as the system is in resonance, the signal is amplified by the maser (bright white spot at $B=B_+$). The cross sections in the frequency domain and over the magnetic field are displayed in the left and bottom sub-plots, respectively. The inset illustrates the setup configuration, a detailed description can be found in Figure S6. **b** Theoretical model of the amplifier: the color represents the expected amplification/attenuation. **c** Measured gain depending on Q-factor, pump power (P_{Laser}) and signal input power (P_{MW}), respectively.

SiC-based refrigerator

Besides using SiC as a coherent microwave source and a low-noise amplifier, this system can also be utilized in reverse as an optically-pumped microwave absorber. This leads to an effective cooling of the microwave mode temperature and can be used as a refrigerator, as described in the following.

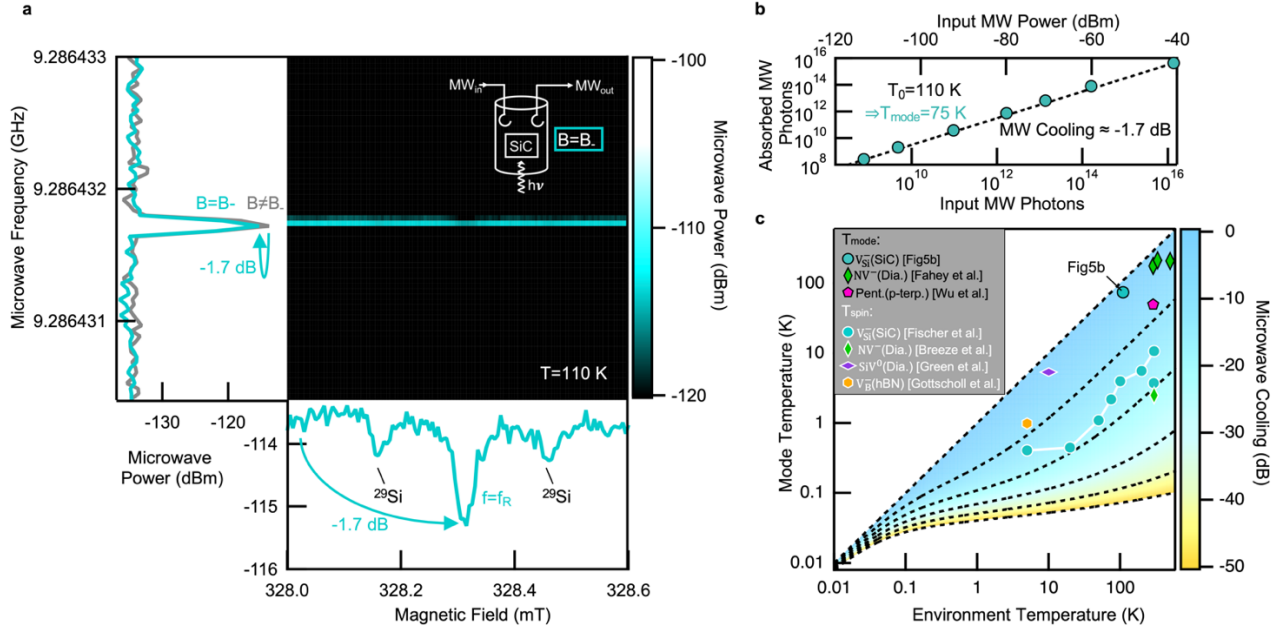


Figure 5: SiC-based refrigerator. **a** Color map of the measured microwaves: a narrow cyan line is given by the inserted microwave signal. As soon as the system is in resonance the signal is attenuated due to induced spin flips of the V_{Si} . The cross sections over frequency and magnetic field are displayed in the left and bottom sub-plots, respectively. The inset illustrates the setup configuration. A detailed description can be found in Figure S6. **b** Measuring the absorbed microwaves for various input powers: a microwave cooling (attenuation) of -1.7dB can be estimated. **c** Simulation of the required microwave cooling to achieve a specific mode temperature for various environmental temperatures. The value of Figure 5b is inserted as well as the data from other publications in order to compare the potential of different material systems (see main text for details).

In order to demonstrate an optically-pumped microwave absorber, we use the same setup as for the amplifier (see Figure 4) but a slightly shifted magnetic field value ($B = B_-$). Since silicon vacancies in SiC possess a $S = 3/2$ spin system, there are three possible ($\Delta m_s = \pm 1$) microwave transitions: B_- , B_0 , B_+ . While the latter transition is emissive and can be used for an amplification of microwaves (as described and used before), the two others are absorptive transitions. The center transition B_0 carries a population difference given by the Boltzmann statistic. Therefore, the spin temperature T_{spin} of this transition is always given by the environmental temperature T_0 . The B_- transition, however, can be optically spin polarized (polarization P) [Fischer et al. 2018, Gottscholl et al. 2022]. This results in a reduced spin temperature lower than the temperature of the environment:

$$T_{spin} = \frac{h\nu}{2k_B \tanh^{-1}(P)} \quad [3]$$

Instead of probing the spin temperature, we can use the polarization to absorb microwave photons, thereby reducing the number of photons in the cavity. Effectively the temperature of a specific microwave mode is reduced to a temperature T_{mode} . To calculate the value, we use Planck's law of blackbody radiation [Rybicki et al. 1919]:

$$B(T) = \frac{2h\nu^3}{c^2} \frac{1}{\exp\left(\frac{h\nu}{k_B T}\right) - 1} \quad [4]$$

We define the microwave cooling (attenuation) C_{dB} according to the gain of an amplifier as the logarithmical ratio of the pristine signal and the modified signal. The number of thermal photons for a specific temperature and frequency is proportional to the spectral radiance $B(T)$. Therefore, the microwave cooling can be described as:

$$C_{dB} = 10 \lg \left(\frac{B(T_{mode})}{B(T_0)} \right) = 10 \lg \left(\frac{\exp\left(\frac{h\nu}{k_B T_0}\right) - 1}{\exp\left(\frac{h\nu}{k_B T_{mode}}\right) - 1} \right) \quad [5]$$

Thus, the mode temperature mainly depends on the measured microwave cooling C_{dB} and the environmental temperature T_0 :

$$T_{mode}(C_{dB}) = \frac{h\nu}{k_B \ln \left(10^{-\frac{C_{dB}}{10}} \left(\exp\left(\frac{h\nu}{k_B T_0}\right) - 1 \right) + 1 \right)} \quad [6]$$

To study this effect and the potential of SiC as a mode cooling device, we insert a microwave signal into the cavity by one antenna and measure the outgoing microwaves after interacting with the spin system with the second antenna. The corresponding color map for a magnetic field sweep over the absorptive transition (B_{-}) is displayed in Figure 5a. Again, the cross sections through the resonance position are displayed in the left and bottom sub-plots, respectively. The attenuation of the signal over the frequency can in fact be barely registered and seems to be in the range of noise. However, since it is a logarithmic scale, the absolute difference at the peak position is more than one order of magnitude larger than the absolute difference at the baseline. Whether this effect originates from the defect can be observed more clearly if the cross-section is set along the incident frequency and the signal is plotted over the magnetic field. In the bottom sub-plot the silicon vacancy transition with its hyperfine peaks can clearly be observed, resulting in an attenuation of -1.7dB (-0.7dB for hyperfine peaks). To address the cooling capability, we varied the microwave power over almost eight orders of magnitude (see Figure 5b). Therefore, we are able to extrapolate the absorbance to the thermal photon basis. As expected, the slope is equal to 1 and the global absorbance (offset of the fit) is -1.7dB. Thus, we can estimate a temperature reduction of $\Delta T = 35 K$ ($\Delta T \approx 15 K$ for hyperfine peak) according to equation [6]. This microwave power-independent absorbance is observable even for high powers (-40dBm) without any saturation effects, highlighting the broad potential of an optically pumped absorber.

Finally, we want to compare the here extracted value of $\Delta T = 35 K$ with other existing systems and discuss the future application but also the limits of this system. Figure 5c summarizes the significant potential of optically pumped refrigerators. The simulation illustrates the required attenuation to achieve a specific mode temperature at various environmental temperatures. We choose a logarithmic scale to cover the regime required for superconducting qubits, which are used in state-of-the-art quantum computers [Arute et al. 2019]. This may be one of the most desirable applications for an optically pumped SiC-based refrigerator. The whole simulation is performed for microwave photons of 9.3 GHz in order to insert the measured value, however, the simulation for other frequencies differs only slightly as shown in Figure S15 (simulation for 1 and 10 GHz). Therefore, it is also possible to insert other results of mode cooling based on different systems such as NV diamond (green diamond) and pentacene (pink pentagon) [Fahey et al. 2022, Wu et al. 2021]. All recently published results are in the same order of magnitude of absorbance and cover a broad range of temperatures. Nevertheless, the potential is much larger, since we can calculate the spin temperature as a limit for the mode temperature. We can use different

spin polarization values of several materials – all possible candidates for optically pumped attenuators (depicted with a white margin). Besides V_{Si}^- in SiC (cyan circle) and NV in diamond (green diamond), we also choose less-common systems such as SiV^0 in diamond (purple diamond) and the boron vacancy (V_B^-) in hexagonal boron nitride (hBN) (orange hexagon) [Green et al. 2017, Gottscholl et al. 2020]. All materials exhibit comparable values and SiC performs well at both, mode temperature and spin temperature. Despite comparable properties, SiC has the highest potential especially in the field of quantum computing. In the following we want to focus on superconducting transmon qubits based on aluminum structures as it is the case for example for Googles sycamore processor [Arute et al. 2019].

Application for quantum computing

In order to realize a transmon qubit, an aluminum line has to be cooled down to 1.2 K to reach superconductivity [Cochran et al. 1958, Jeffrey et al. 2014]. However, in practice the system is cooled down into the mK regime to suppress thermal photons. By replacing the silicon substrate with an irradiated silicon carbide substrate, a mK cooling can be avoided since the suppressing of thermal photons can be achieved by the V_{Si}^- cooling effect within the substrate. Since the qubits are also in the GHz regime, the required magnetic field values are quite comparable to the values mentioned in this paper. (Local) optical pumping results in an absorbance of the microwaves and therefore, the resonator can be “cooled” before starting the initialization procedure of the qubit. Here, the optical pumping should not be critical to the <1 K devices, since much lower optical power is required in this temperature range. To reach the required spin polarization, the pump rate has to be in the order of the spin lattice relaxation rate which depends strongly on the temperature for SiC [Simin et al. 2017]. Therefore, only a few μW of laser power ($P_{Laser} \sim T_0^{-5}$) are required to reach a sufficient spin polarization, which should not affect the critical temperature of the superconducting aluminum. One of the most important aspects of a quantum computer and its qubits is a precise readout of the states. In state-of-the-art quantum computers this is realized by a state-dependent detuning of the resonance frequency of a readout resonator [Jeffrey et al. 2014]. The tiny signal needs to be amplified by 100dB with a cascade of low-noise amplifiers in order to reach power levels high enough to exceed the thermal background outside of the cryostat where the experimental hardware is located. The quality of the LNAs is the limiting component to distinguish between different quantum states of the qubit. Here, we propose to use a SiC-based amplifier as the first low-noise pre-amplifier. A simple switching of the magnetic field results in an enhanced readout of the system by tuning the resonance of the silicon vacancies to the same frequency as the readout resonator. In this context, we want to highlight that a unique feature of the silicon vacancy is the very small zero-field splitting parameter. This results in a very small required magnetic field (± 2.5 mT) to switch between the refrigerator and the amplifier. NV diamond is not applicable for an easy switchable amplifier/refrigerator device since magnetic fields of ± 102.5 mT are required. The magnetic field can also be used for tuning the resonance frequency of flux/squid-based qubits [Paauw et al. 2009, Kim et al. 2019,], thus, even the ± 2.5 mT for the V2 defect might be critical. Here, we want to highlight that SiC hosts a large variety of defects with different zero-field splittings which can be chosen depending on the application. As an example, we demonstrate in Figure S16 that the V1 defect shows emission/absorption properties comparable to those of the here-studied V2 defect. Therefore, a similar maser

device can be realized using the V1 defect with the advantage that switching between amplifier/refrigerator requires only $\pm 163 \mu\text{T}$.

Conclusion

In summary, our study marks a significant milestone by introducing the first continuous-wave SiC-based maser. Employing an innovative feedback loop, we successfully enhance the Q-factor, enabling precise control of critical parameters necessary for a robust and coherent microwave source, even beyond room temperature. Through comprehensive simulations, we underscore the vast potential inherent in the SiC-based maser technology. Furthermore, our research showcases SiC's remarkable low-noise preamplification capability, achieving an impressive 10dB amplification in these initial proof-of-concept studies. Additionally, our demonstration of SiC's capacity for microwave mode cooling and its potential integration with quantum computers employing transmon qubits is promising for future technological advancements. Given SiC's established presence in the industry and its scalability for large-scale production, our findings amplify the transformative potential of SiC in contemporary microwave technologies. This breakthrough heralds a new era in maser-based applications, paving the way for innovative advancements and practical implementations across various fields.

References

[Anisimov et al. 2016]: Anisimov, A. N., Simin, D., Soltamov, V. A., Lebedev, S. P., Baranov, P. G., Astakhov, G. V., & Dyakonov, V. (2016). Optical thermometry based on level anticrossing in silicon carbide. *Scientific reports*, 6(1), 1-5.

[Arroo et al. 2021]: Arroo, D. M., Alford, N. M., & Breeze, J. D. (2021). Perspective on room-temperature solid-state masers. *Applied Physics Letters*, 119(14), 140502. doi: 10.1063/5.0061330

[Arute et al. 2019]: Arute, F., Arya, K., Babbush, R., Bacon, D., Bardin, J. C., Barends, R., Biswas, R., Boixo, S., Brandao, F. G., Buell, D. A., Burkett, B., Chen, Y., Chen, Z., Chiaro, B., Collins, R., Courtney, W., Dunsworth, A., Farhi, E., Foxen, B., Fowler, A., Gidney, C., Giustina, M., Graff, R., Guerin, K., Habegger, S., Harrigan, M. P., Hartmann, M. J., Ho, A., Hoffmann, M., Huang, T., Humble, T. S., Isakov, S. V., Jeffrey, E., Jiang, Z., Kafri, D., Kechedzhi, K., Kelly, J., Klimov, P. V., Knysh, S., Korotkov, A., Kostritsa, F., Landhuis, D., Lindmark, M., Lucero, E., Lyakh, D., Mandrà, S., McClean, J. R., McEwen, M., Megrant, A., Mi, X., Michielsen, K., Mohseni, M., Mutus, J., Naaman, O., Neeley, M., Neill, C., Niu, M. Y., Ostby, E., Petukhov, A., Platt, J. C., Quintana, C., Rieffel, E. G., Roushan, P., Rubin, N. C., Sank, D., Satzinger, K. J., Smelyanskiy, V., Sung, K. J., Trevithick, M. D., Vainsencher, A., Villalonga, B., White, T., Yao, Z. J., Yeh, P., Zalcman, A., Neven, H. and Martinis, J. M. (2019). Quantum supremacy using a programmable superconducting processor. *Nature*, 574(7779), 505-510.

[Breeze et al. 2015]: Breeze, J., Tan, K. J., Richards, B., Sathian, J., Oxborrow, M., & Alford, N. M. (2015). Enhanced magnetic Purcell effect in room-temperature masers. *Nature Communications*, 6(1), 1-6. doi: 10.1038/ncomms7215 (2015)

- [Breeze et al. 2017]: Breeze, J. D., Salvadori, E., Sathian, J., Alford, N. M., & Kay, C. W. (2017). Room-temperature cavity quantum electrodynamics with strongly coupled Dicke states. *npj Quantum Information*, 3(1), 1-5. doi: 10.1038/s41534-017-0041-3
- [Breeze et al. 2018]: Breeze, J. D., Salvadori, E., Sathian, J., Alford, N. M., & Kay, C. W. (2018). Continuous-wave room-temperature diamond maser. *Nature*, 555(7697), 493-496. doi: 10.1038/nature25970
- [Carter et al. 2015]: Carter, S. G., Soykal, Ö. O., Dev, P., Economou, S. E., & Glaser, E. R. (2015). Spin coherence and echo modulation of the silicon vacancy in 4 H- SiC at room temperature. *Physical Review B*, 92(16), 161202.
- [Cochran et al. 1958]: Cochran, J. F., & Mapother, D. E. (1958). Superconducting transition in aluminum. *Physical Review*, 111(1), 132.
- [Fahey et al. 2022]: Fahey, D. P., Jacobs, K., Turner, M. J., Choi, H., Hoffman, J. E., Englund, D., & Trusheim, M. E. (2022). Steady-state microwave mode cooling with a diamond NV ensemble. arXiv preprint arXiv:2203.03462.
- [Fischer et al. 2018]: Fischer, M., Sperlich, A., Kraus, H., Ohshima, T., Astakhov, G. V., & Dyakonov, V. (2018). Highly efficient optical pumping of spin defects in silicon carbide for stimulated microwave emission. *Physical Review Applied*, 9(5), 054006. doi: 10.1103/PhysRevApplied.9.054006
- [Gordon et al. 1955]: Gordon, J. P., Zeiger, H. J., & Townes, C. H. (1955). The maser—new type of microwave amplifier, frequency standard, and spectrometer. *Physical review*, 99(4), 1264.
- [Gottscholl et al. 2020]: Gottscholl, A., Kianinia, M., Soltamov, V., Orlinskii, S., Mamin, G., Bradac, C., Kasper, C., Krambrock, K., Sperlich, A., Toth, M., Aharonovich, I., & Dyakonov, V. (2020). Initialization and read-out of intrinsic spin defects in a van der Waals crystal at room temperature. *Nature Materials*, 19(5), 540-545. doi: 10.1038/s41563-020-0619-6
- [Gottscholl et al. 2022]: Gottscholl, A., Wagenhöfer, M., Klimmer, M., Scherbel, S., Kasper, C., Baianov, V., Astakhov, G. V., Dyakonov, V. and Sperlich, A. (2022). Superradiance of Spin Defects in Silicon Carbide for Maser Applications. *Front. Photonics* 3:886354. doi: 10.3389/fphot.2022.886354
- [Green et al. 2017]: Green, B. L., Mottishaw, S., Breeze, B. G., Edmonds, A. M., D’Haenens-Johansson, U. F. S., Doherty, M. W., Williams, S. D., Twitchen, D.J. and Newton, M. E. (2017). Neutral silicon-vacancy center in diamond: Spin polarization and lifetimes. *Physical review letters*, 119(9), 096402.
- [Jeffrey et al. 2014]: Jeffrey, E., Sank, D., Mutus, J. Y., White, T. C., Kelly, J., Barends, R., Chen, Y., Chen, Z., Chiaro, B., Dunsworth, A., Megrant, A., O’Malley, P. J. J., Neill, C., Roushan, P., Vainsencher, A., Wenner, J., Cleland, A. N. and Martinis, J. M. (2014). Fast accurate state measurement with superconducting qubits. *Physical review letters*, 112(19), 190504.
- [Jiang et al. 2021]: Jiang, M., Su, H., Wu, Z., Peng, X., & Budker, D. (2021). Floquet maser. *Science Advances*, 7(8), eabe0719.

- [Jin et al. 2015]: Jin, L., Pfender, M., Aslam, N., Neumann, P., Yang, S., Wrachtrup, J., & Liu, R. B. (2015). Proposal for a room-temperature diamond maser. *Nature Communications*, 6(1), 1-8. doi: 10.1038/ncomms9251
- [Kawahito et al. 2018]: Kawahito, Y., Wang, H., Katayama, S., & Sumimori, D. (2018). Ultra high power (100 kW) fiber laser welding of steel. *Optics letters*, 43(19), 4667-4670.
- [Kim et al. 2019]: Kim, S., Shrekenhamer, D., McElroy, K., Strikwerda, A., & Alldredge, J. (2019). Tunable superconducting cavity using superconducting quantum interference device metamaterials. *Scientific Reports*, 9(1), 1-9.
- [Kleppner et al. 1962]: Kleppner, D., Goldenberg, H. M., & Ramsey, N. F. (1962). Theory of the hydrogen maser. *Physical Review*, 126(2), 603.
- [Konoplev et al. 2006]: Konoplev, I. V., McGrane, P., He, W., Cross, A. W., Phelps, A. D. R., Whyte, C. G., Ronald, K. and Robertson, C. W. (2006). Experimental study of coaxial free-electron maser based on two-dimensional distributed feedback. *Physical review letters*, 96(3), 035002.
- [Kraus et al. 2014]: Kraus, H., Soltamov, V. A., Riedel, D., V ath, S., Fuchs, F., Sperlich, A., Baranov, P. G., Dyakonov, D. & Astakhov, G. V. (2014). Room-temperature quantum microwave emitters based on spin defects in silicon carbide. *Nature Physics*, 10(2), 157-162. doi: 10.1038/nphys2826
- [Lamb et al. 1964]: Lamb Jr, W. E. (1964). Theory of an optical maser. *Physical Review*, 134(6A), A1429.
- [Lekavicius et al. 2022]: Lekavicius, I., Myers-Ward, R. L., Pennachio, D. J., Hajzus, J. R., Gaskill, D. K., Purdy, A. P., Yeats, A.L. Brereton, P. G., Glaser, E. R., Reinecke, T. L. and Carter, S. G. (2022). Orders of Magnitude Improvement in Coherence of Silicon-Vacancy Ensembles in Isotopically Purified 4 H-SiC. *PRX Quantum*, 3(1), 010343.
- [Lesage et al. 1981]: Lesage, P., & Audoin, C. (1981). Frequency stability of an oscillating maser: Analysis of the effect of an external feedback loop. *IEEE Transactions on Instrumentation and Measurement*, (3), 182-186.
- [Ng et al. 2023]: Ng, W., Wen, Y., Attwood, M., Jones, D.C., Oxborrow, M., Alford, N.M. and Arroo, D.M., 2023. Maser-in-a-Shoebbox': a portable plug-and-play maser device at room-temperature and zero magnetic-field. *arXiv preprint arXiv:2310.09269*.
- [Orlinski et al. 2003]: Orlinski, S. B., Schmidt, J., Mokhov, E. N., & Baranov, P. G. (2003). Silicon and carbon vacancies in neutron-irradiated SiC: A high-field electron paramagnetic resonance study. *Physical Review B*, 67(12), 125207. doi: 10.1103/PhysRevB.67.125207
- [Oxborrow et al. 2012]: Oxborrow, M., Breeze, J. D., & Alford, N. M. (2012). Room-temperature solid-state maser. *Nature*, 488(7411), 353-356.
- [Paauw et al. 2009]: Paauw, F. G., Fedorov, A., Harmans, C. M., & Mooij, J. E. (2009). Tuning the gap of a superconducting flux qubit. *Physical review letters*, 102(9), 090501.
- [Rodriguez et al. 2023]: Rodriguez, C.B., 2023. Room-temperature solid-state masers as low-noise amplifiers to facilitate deep-space missions using small spacecraft. *arXiv preprint arXiv:2308.00848*.

- [Rybicki et al. 1991]: Rybicki, G. B., & Lightman, A. P. (1991). Radiative processes in astrophysics. John Wiley & Sons.
- [Siegman et al. 1964]: Siegman, A. E., Quate, C. F., Bjorkholm, J., & Francois, G. (1964). Frequency Translation of an He–Ne Laser's Output Frequency by Acoustic Output Coupling Inside the resonant Cavity. *Applied Physics Letters*, 5(1), 1-2.
- [Simin et al. 2016]: Simin, D., Soltamov, V. A., Poshakinskiy, A. V., Anisimov, A. N., Babunts, R. A., Tolmachev, D. O., Mokhov, E. N., Trupke, M., Tarasenko, S. A., Sperlich, A., Baranov, P. G., Dyakonov, V. and Astakhov, G. V. (2016). All-optical dc nanotesla magnetometry using silicon vacancy fine structure in isotopically purified silicon carbide. *Physical Review X*, 6(3), 031014.
- [Simin et al. 2017]: Simin, D., Kraus, H., Sperlich, A., Ohshima, T., Astakhov, G. V., & Dyakonov, V. (2017). Locking of electron spin coherence above 20 ms in natural silicon carbide. *Physical Review B*, 95(16), 161201. doi: 10.1103/PhysRevB.95.161201
- [Udem et al. 2002]: Udem, T., Holzwarth, R., & Hänsch, T. W. (2002). Optical frequency metrology. *Nature*, 416(6877), 233-237.
- [Wu et al. 2020]: Wu, H., Xie, X., Ng, W., Mehanna, S., Li, Y., Attwood, M., & Oxborrow, M. (2020). Room-temperature quasi-continuous-wave pentacene maser pumped by an invasive Ce: YAG luminescent concentrator. *Physical Review Applied*, 14(6), 064017.
- [Wu et al. 2021]: Wu, H., Mirkhanov, S., Ng, W., & Oxborrow, M. (2021). Bench-Top Cooling of a Microwave Mode Using an Optically Pumped Spin Refrigerator. *Physical Review Letters*, 127(5), 053604.
- [Wu H et al. 2023]: Wu, H., Yang, S., Oxborrow, M., Jiang, M., Zhao, Q., Budker, D., Zhang, B. and Du, J., 2022. Enhanced quantum sensing with room-temperature solid-state masers. *Science Advances*, 8(48), eade1613.
- [Wu Q et al. 2023]: Wu, Q., Zhang, Y., Wu, H., Su, S.L., Liu, K.K., Oxborrow, M., Shan, C. and Mølmer, K., 2022. Superradiant Masing with Solid-state Spins at Room Temperature. arXiv preprint arXiv:2212.01864.
- [Zollitsch et al. 2023]: Zollitsch, C.W., Ruloff, S., Fett, Y., Wiedemann, H.T., Richter, R., Breeze, J.D. and Kay, C.W., 2023. Maser Threshold Characterization by Resonator Q-Factor Tuning. arXiv preprint arXiv:2302.10811.

Acknowledgement

This research was funded by the European Research Council (ERC) (Grant agreement No. 101055454) and the German Research Foundation DFG (DFG-DY 18/13-1). A.G., V.B., A.S., and V.D. acknowledge financial support from the DFG through the Würzburg-Dresden Cluster of Excellence on Complexity and Topology in Quantum Matter - ct.qmat (EXC 2147, project-id 39085490). The study was supported by the Jet Propulsion Laboratory, California Institute of Technology, under contract with the National Aeronautics and Space Administration (contract 80NM0018D0004).

Author information

Authors and Affiliations

NASA Jet Propulsion Laboratory, California Institute of Technology, Pasadena, California, USA

Andreas Gottscholl

Experimental Physics 6 and Würzburg-Dresden Cluster of Excellence ct.qmat, Julius-Maximilians-Universität Würzburg, 97074 Würzburg, Germany

Andreas Gottscholl, Maximilian Wagenhöfer, Valentin Baianov, Vladimir Dyakonov, Andreas Sperlich

Contributions

A.G., M.W. and A.S. designed and realized the home-made spectrometer. A.G. and M.W. performed theoretical calculations of the relevant parameters affecting the maser threshold and performed all measurements. V.B. designed the microwave resonator which was characterized by A.G.. A.G., V.D. and A.S. wrote the manuscript. A.S. conceived the idea and supervised the project together with A.G.. All authors discussed the results and commented on the manuscript.

Supplementary Information

for:

Room-Temperature Silicon Carbide Maser: Unveiling Quantum Amplification and Cooling

Andreas Gottscholl^{1,2,a)}, Maximilian Wagenhöfer¹, Valentin Baianov¹, Vladimir Dyakonov¹,
Andreas Sperlich^{1,b)}

¹Experimental Physics 6 and Würzburg-Dresden Cluster of Excellence ct.qmat,
Julius-Maximilians-Universität Würzburg, 97074 Würzburg, Germany

²NASA Jet Propulsion Laboratory, California Institute of Technology, Pasadena, California,
USA

a) Electronic mail: andreas.p.gottscholl@jpl.nasa.gov

b) Electronic mail: andreas.sperlich@uni-wuerzburg.de

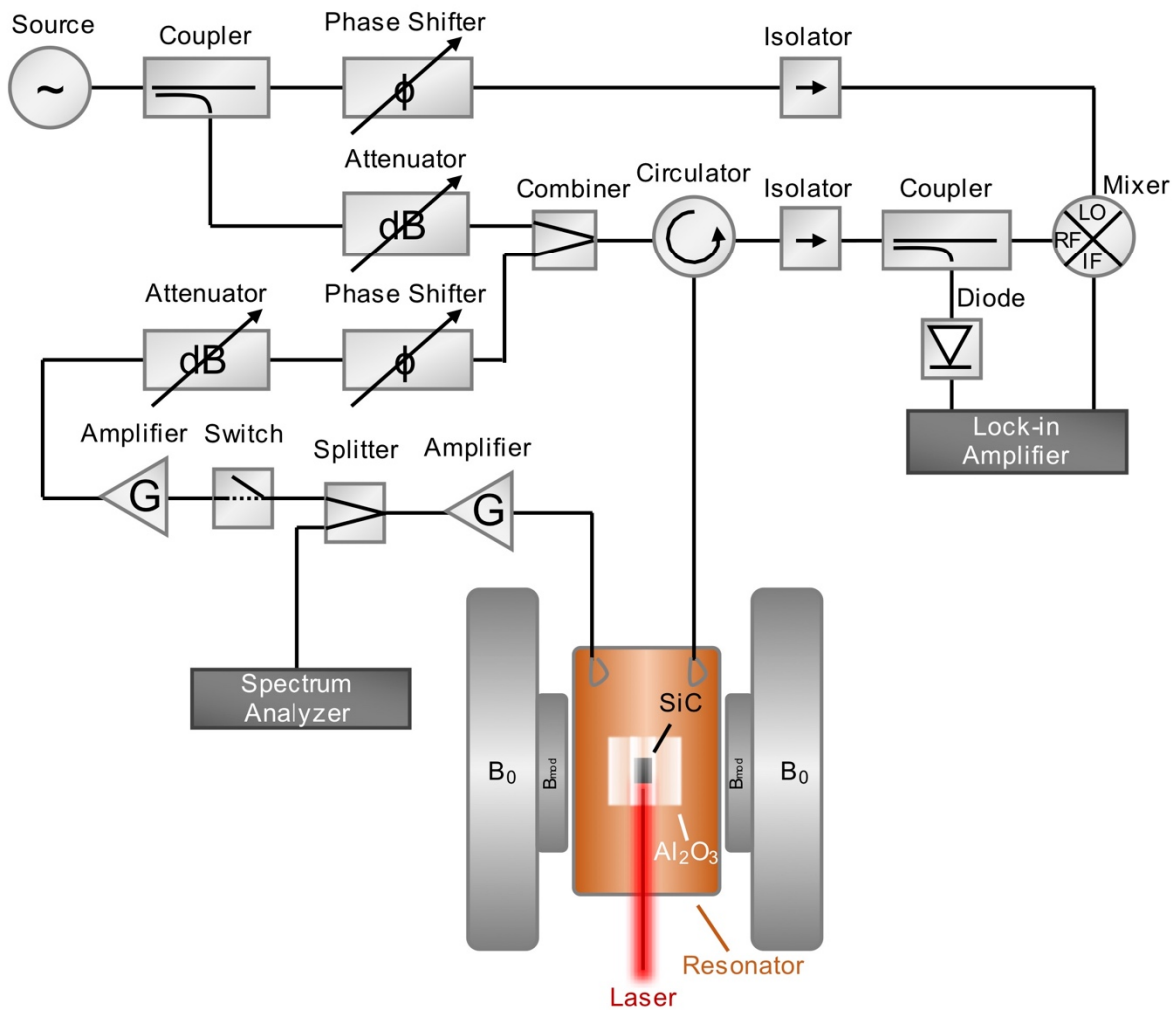


Figure S1: Self-built setup for Q-factor, electron paramagnetic resonance, (Q-boosted) maser, amplifier and refrigerator measurements.

Setup Details

The main results of this work were all recorded with one single self-built setup. Since the here-reported microwave bridge enables six different modes of operation, we will focus on the different signal paths separately for each measurement in the next sections. The whole setup is illustrated in Figure S1. As a microwave source we used an *Anritsu MG 3694C*. Most of the components are commercially available: As coupler we used a -10dB *Mini-Circuits ZUDC10-02183-S+* (left) and a -20dB *Radiall R433724700* (right). The isolators *Aerotek I2E1L1FF* are integrated to block unwanted microwave reflections. For combiner/splitter we used *Mini-Circuits ZFRSC-183-S+*, while the detection is performed with a detector diode *Advanced Control Components ACTP-1504P*, a mixer *Marki M10412LA*, a lock-in amplifier *Signal Recovery 7230* and a spectrum analyzer *WSA 5000* (see the following section for detailed measurement explanations). To compensate microwave losses, we used a *Miteq AFS4.08001200-10.200* LNA (right) and a *Narda N62448-243* (left). A microwave switch *Mini-Circuits MSP2TA-18-12+* as well as two modified Rotary Vane attenuators with added servo motors are controlled via an *Arduino*. For phase corrections we used two analog phase shifters from an old *Bruker E300* microwave bridge, which are controlled via the DAC of the lock-in amplifier. For optical pumping we used an 808 nm-laser *K808FANFA-15.00W* from *BWT* which provides a variable power of 0-15000 mW.

Q-factor measurement:

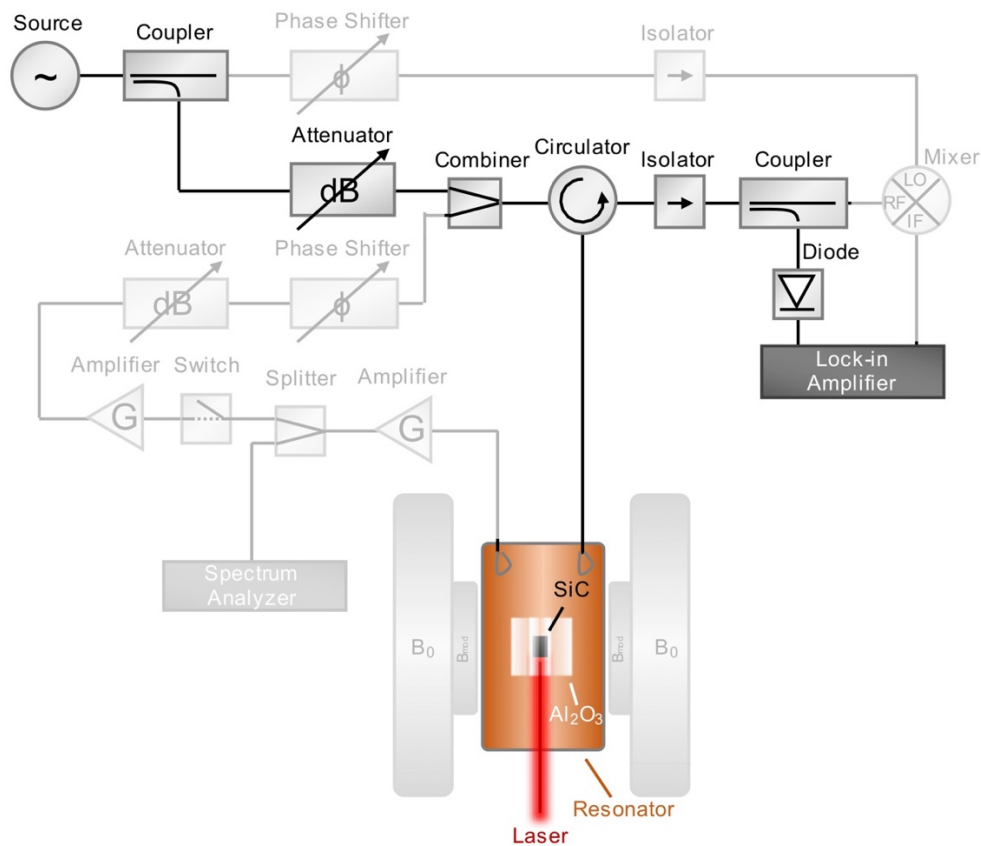


Figure S2: Setup for Q-factor measurements: the microwave frequency is swept while the output is on/off-modulated. The reflected microwave power is measured via a detector diode and a lock-in amplifier.

The basis for all measurements reported in this paper is the determination of the Q-factor of the resonator and in particular its resonance frequency. This is accomplished by sweeping the frequency of an inserted microwave probe while measuring the reflected microwave power. Via a circulator the reflected microwaves are separated from the inserted microwaves and detected with a detector diode. Since the measurement provides a very high signal-to-noise ratio only a very small amount of the signal is required. Thus, we use a coupler with -20dB which transmits most of the signal for the EPR measurement (see next section). The detection of the small signal is realized with a lock-in amplifier. We choose an on/off modulation of the microwaves in order to observe the reflection directly, which results in a quantitative analysis of the Lorentzian dip providing information about under/over-coupling or critical coupling of the resonator (see Figure S9). This calibration routine for the maser/amplifier/refrigerator is performed with an active laser output since a small heating leads to a drift of the resonance frequency. Thus, we start with further measurements as soon as the Q-factor measurements reveals a stable resonance frequency.

Electron Paramagnetic Resonance:

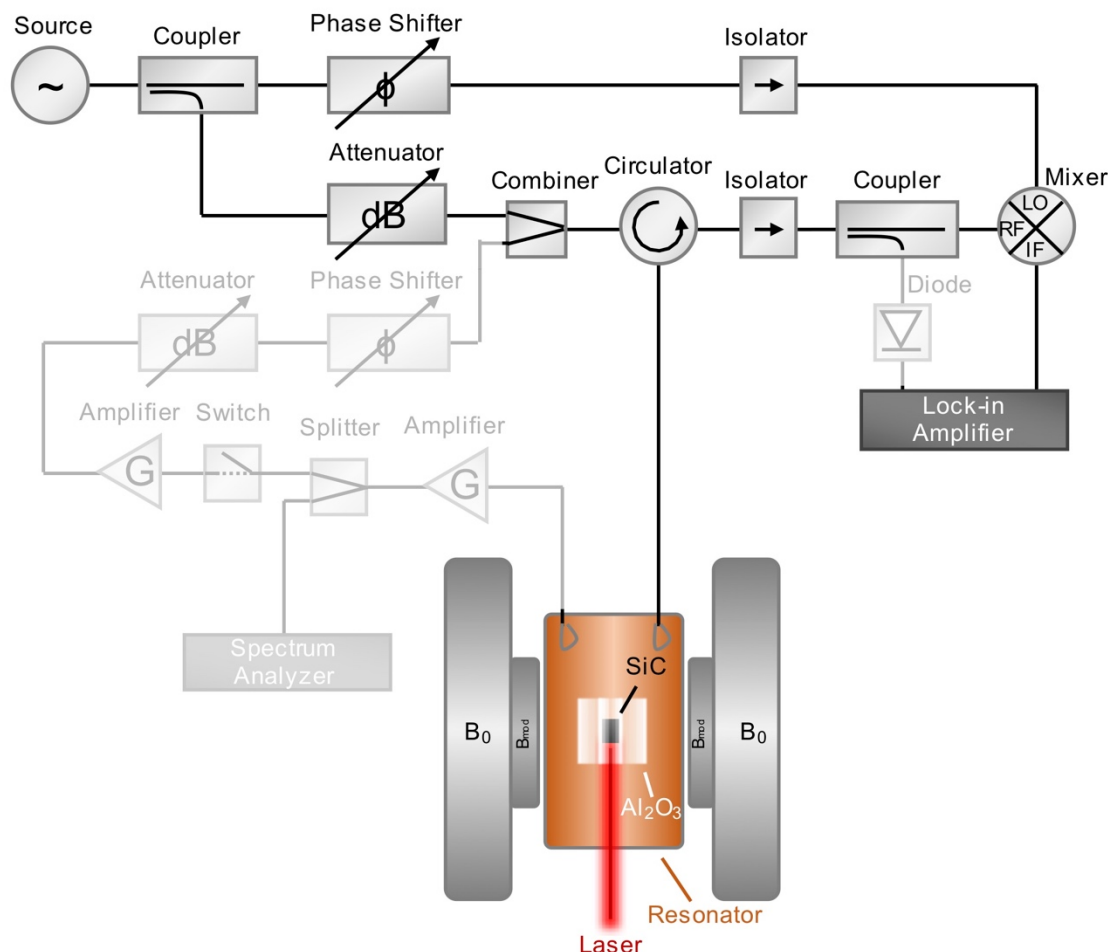


Figure S3: Setup for electron paramagnetic resonance: The microwave frequency is fixed to the resonance frequency of the resonator. The main part of the microwaves drives phase-adjusted the local oscillator of a mixer. A small part is attenuated to a sufficiently low power and interacts with the sample. The remaining microwaves are detected via the mixer and the lock-in amplifier.

With the previous measurement we extracted the correct frequency regime ($f \approx f_R$). Besides the frequency, a maser/amplifier/refrigerator requires also the correct magnetic field range ($B \approx B_{\pm}$). A perfect measurement for probing the resonance condition of the spin system is electron paramagnetic resonance (EPR). Again, the microwave reflection is measured, but the swept quantity is the magnetic field using a pair of Helmholtz coils (see Figure S3). The microwave output is fixed to the resonance frequency f_R in a continuous wave mode. To enhance the signal-to-noise ratio we are using the same lock-in amplifier (second input), and the magnetic field is sinusoidally modulated with a pair of small modulation coils. The interacting microwaves are attenuated (0-60dB) to avoid saturation of the spin system.

The main part of the microwaves is guided through the first coupler to drive the local oscillator of the mixer. A phase shifter is implemented to phase-adjust the microwaves, thus providing the correct phase of the down-converted intermediate frequency. The remaining down-converted frequency is identical to the modulation frequency and recorded by the lock-in amplifier. Besides the information of the resonant magnetic field ($B \approx B_{\pm}$), EPR reveals the spin polarization of the system (see [Fischer et al. 2018] and [Gottscholl et al. 2020] for details). Thus, the pump threshold for the maser can be estimated with EPR.

Maser:

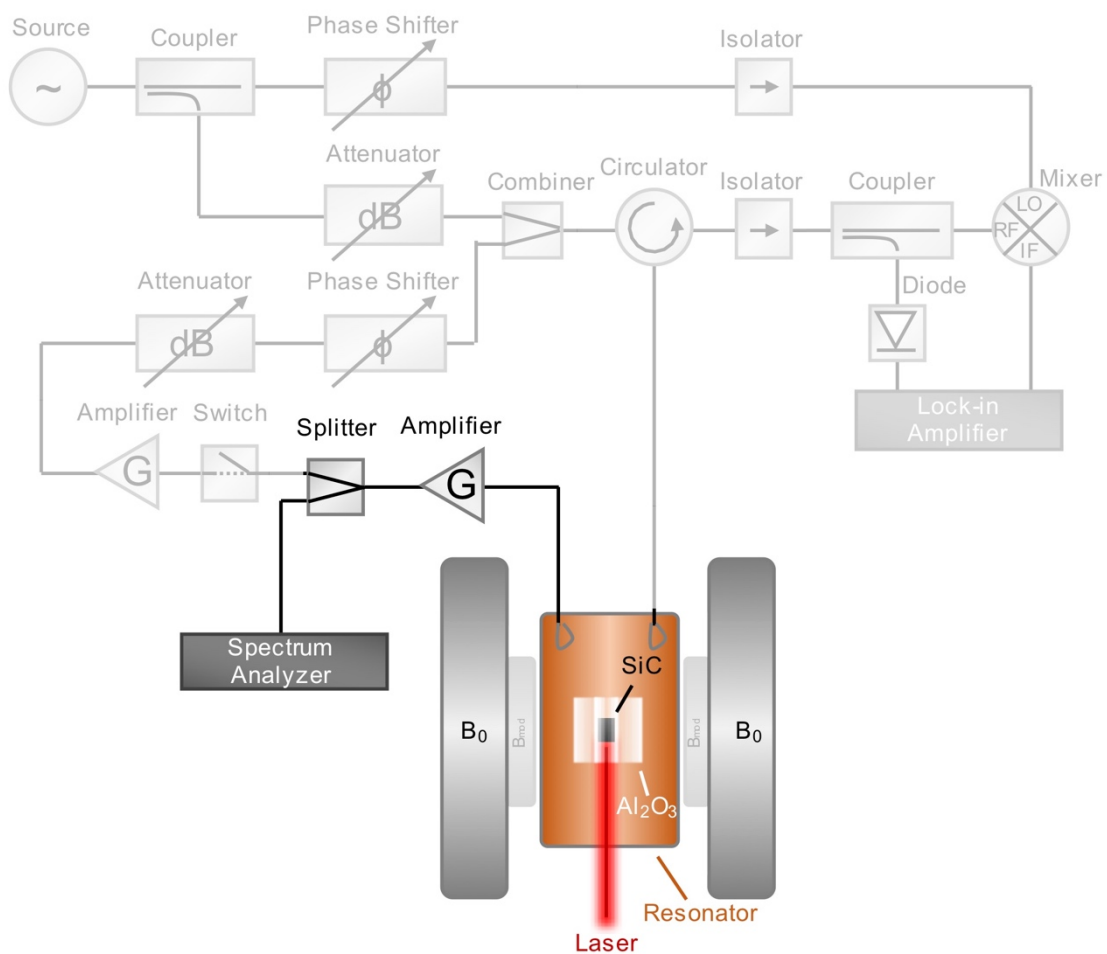


Figure S4: Setup for maser measurements: The sample is excited via a laser within an external magnetic field. The emitted microwaves are amplified (to compensate losses) and guided to a spectrum analyzer.

For the maser output measurement, the magnetic field range is arranged according to the previous EPR experiment and the frequency range of the recording spectrum analyzer is adjusted to the resonance frequency of the resonator. To compensate several losses (e.g. inserted splitter for the next measurement type), a LNA is inserted.

Q-boosted Maser:

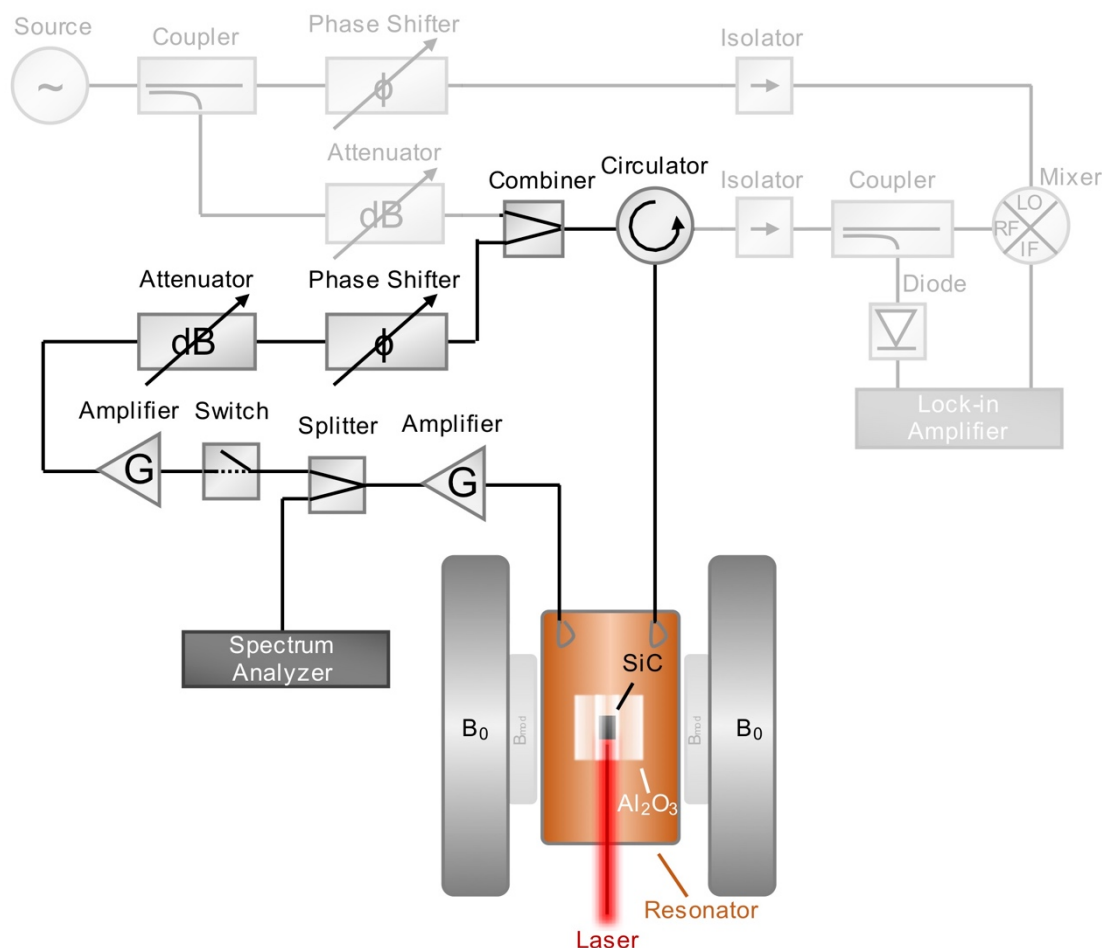


Figure S5: Setup for Q-boosted maser measurements: By closing the microwave switch, the feed-back loop can be activated. After amplification (+attenuation) and phase adjustment the microwaves are inserted back into the resonator. Only a part of the signal is guided to the spectrum analyzer.

The artificial enhancement of the Q-factor is realized by a feed-back loop. The Q-boosting is activated by closing the microwave switch. 50% of the output signal after the LNA are amplified by a second amplifier. To avoid an overdrive the gain is controlled by attenuating (0-60dB) the previously amplified signal. After phase adjustment via a phase shifter, the microwaves are inserted back into the resonator.

Amplifier/Refrigerator:

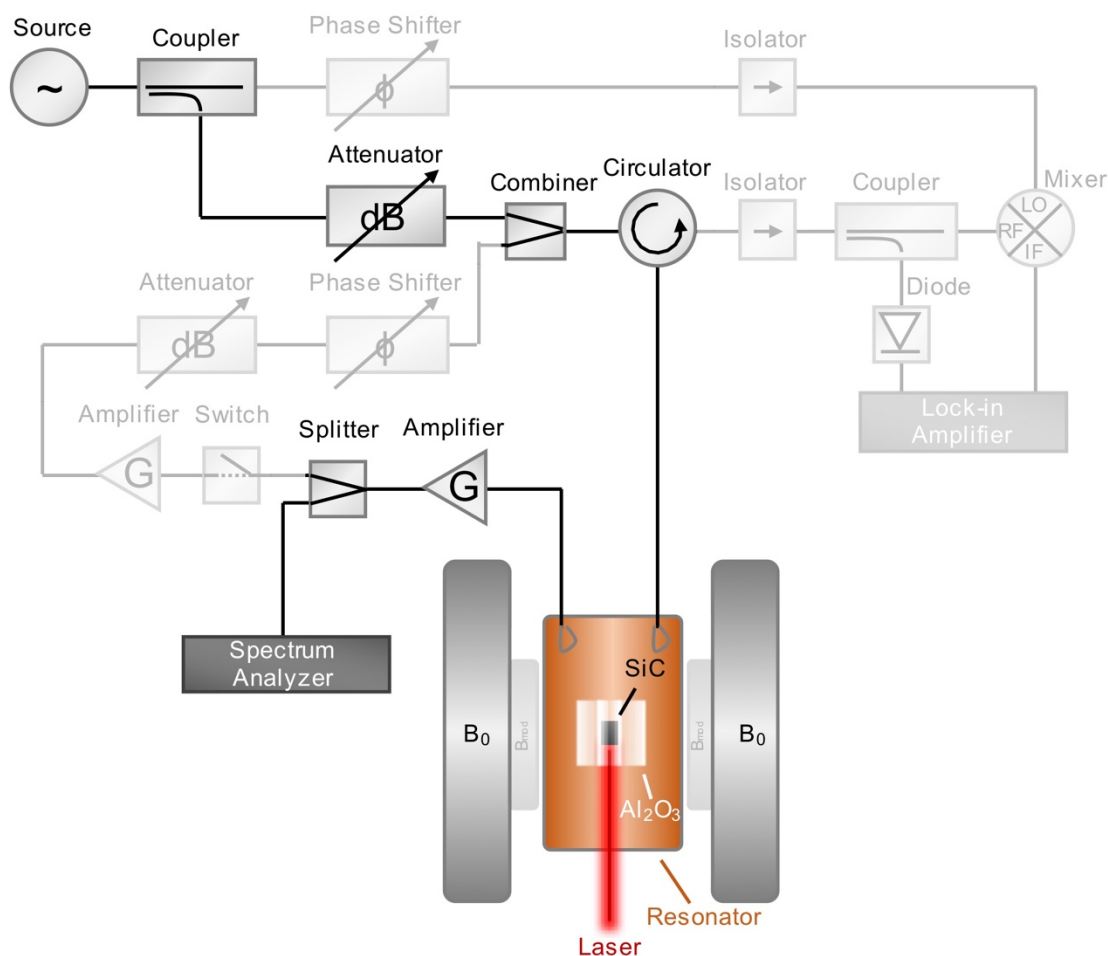


Figure S6: Setup for amplifier/refrigerator measurements: an arbitrary microwave signal is inserted into the resonator by one antenna. A second antenna detects the output signal. The amplifier (refrigerator) can be switched on for $B = B_+$ ($B = B_-$) and off for $B \neq B_+$ ($B \neq B_-$), respectively.

The amplifier and refrigerator are analyzed by inserting a test signal into the system. The frequency is adjusted to the resonance frequency and the magnetic field within the range of the resonant condition. The amplifier (refrigerator) can be switched off by an off-resonance magnetic field $B \neq B_+$ ($B \neq B_-$). As soon as the magnetic field is in the range of the resonance condition $B = B_+$ ($B = B_-$), the spin system interacts with the microwaves and the amplification (absorption) is recorded with the spectrum analyzer.

Resonator Design

Different parameters were varied iteratively to find the most suitable resonator for the maser/amplifier/refrigerator. We started with an empty brass and copper resonator with dielectric sapphire core and compared the influence of conductance on the Q-factor (see Figure S7). As expected, the copper resonator provides a higher value. Therefore, we continued with height-dependent measurements (see Figure S8 a and b). Here, we already included the gain material to find the best constellation for a SiC-based device. We further changed the diameter of the resonator with the highest Q-factor from the height-dependent measurements to get the highest value of $Q=17600$ (see Figure S8). To increase the Q-factor even more we can either under couple the system or cool down the resonator to

reduce ohmic losses (see Figure S9). The highest value of $Q_{\max}=85000$ was reached for a temperature of $T=87$ K. This was approximately the lowest possible temperature of the liquid nitrogen cryostat, since the whole ensemble has to be cooled resulting in thermal losses. However, as soon as the laser is activated the temperature stabilizes around $T=110$ K.

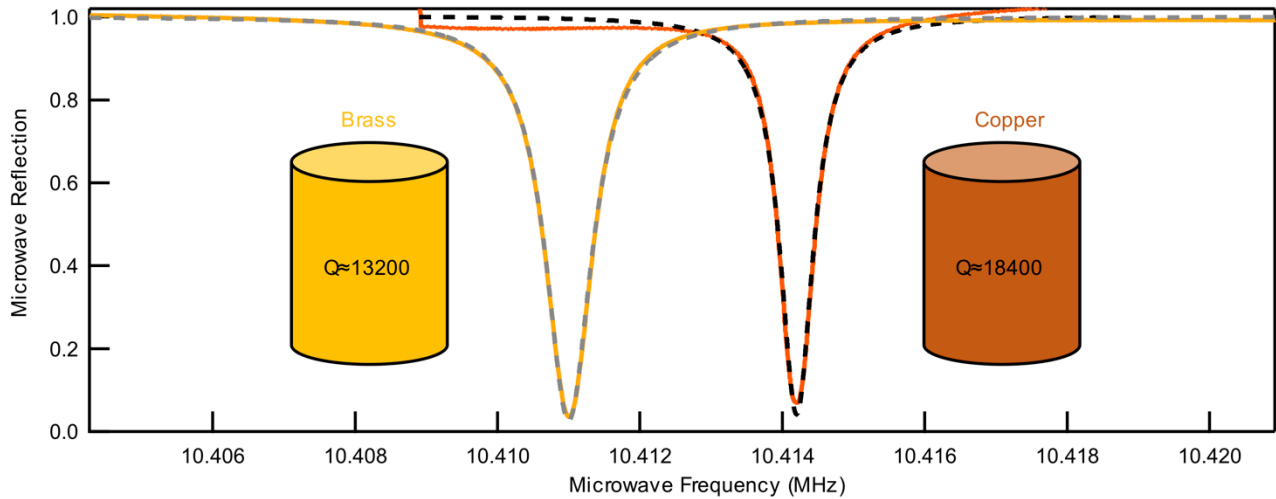


Figure S7: Influence of the resonator material on the quality of the resonator: Due to the higher conductivity the ohmic losses are reduced in a copper resonator in comparison to a brass resonator with identical dimensions. The Q-factor values are shown here for an empty cavity (with sapphire, but without silicon carbide).

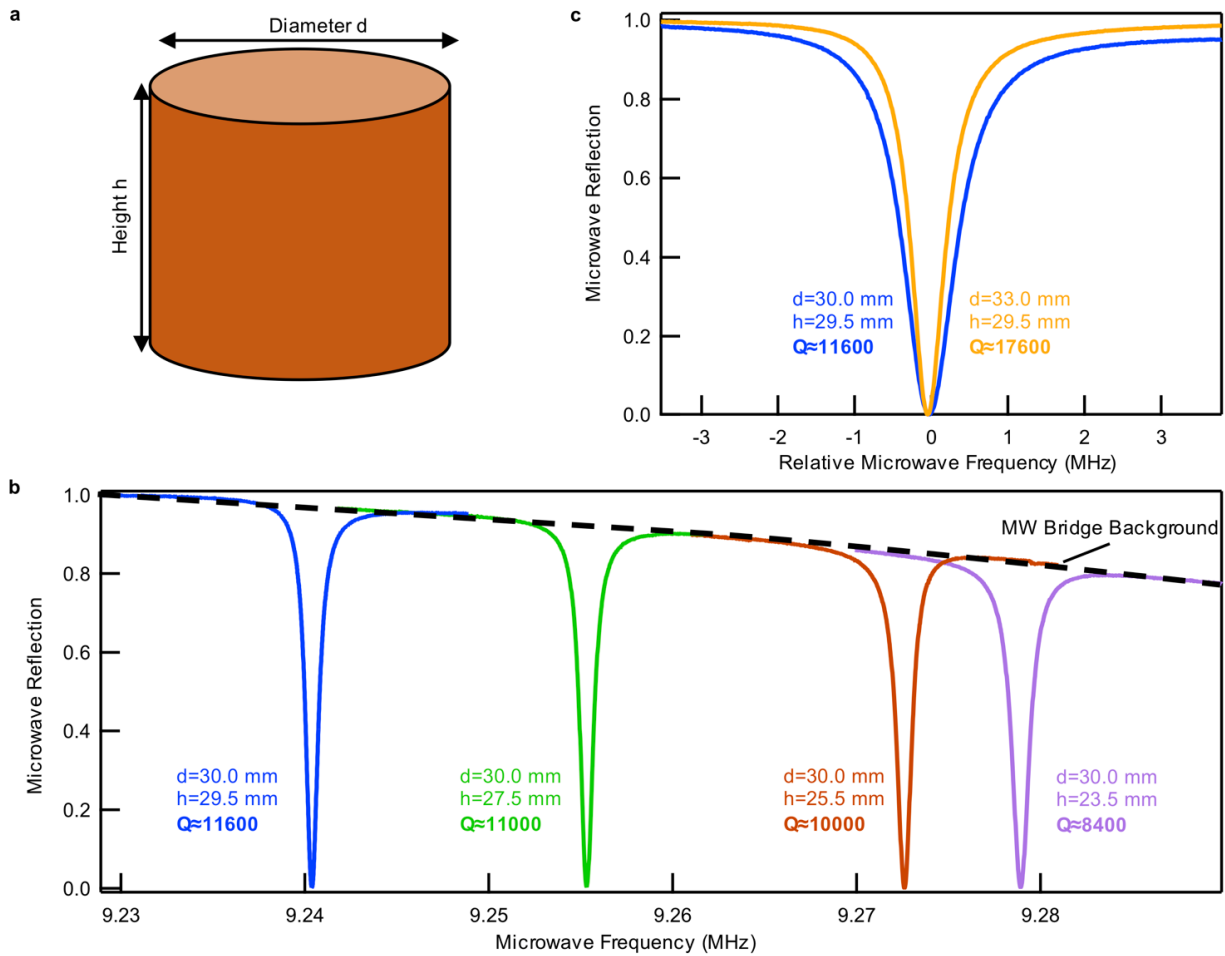


Figure S8. Influence of the resonator dimensions on the Q-factor: **a** The height h is varied as well as the diameter d of the copper resonator filled with silicon carbide in order to find the highest Q-factor. **b** First, the height is varied. With increasing height, the resonance frequency shifts towards lower frequencies (absorption due to the microwave bridge background is indicated with a dashed line). **c** We chose the resonator with the highest Q-factor and enhanced the value by changing the diameter (relative frequency used due to large resonance frequency shift of 78 MHz).

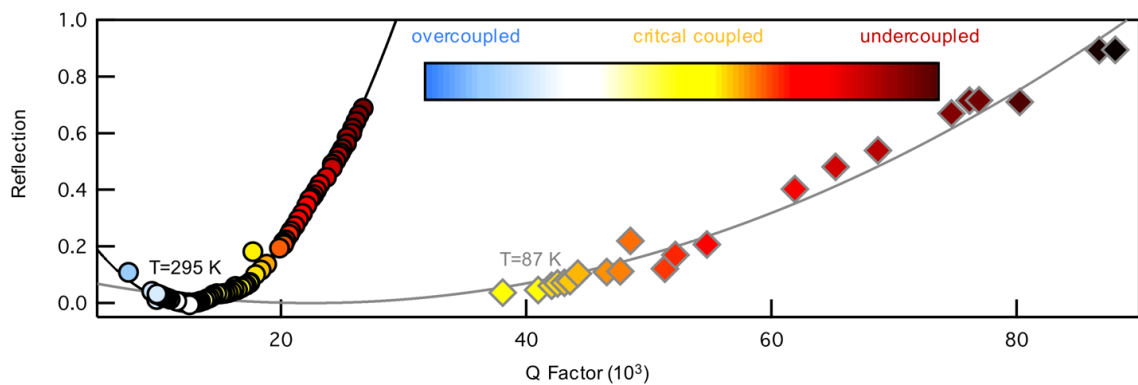


Figure S9. Quality factor variation of the resonator without feedback loop: The Q-factor can be varied slightly by moving the coupling antenna in and out of the resonator. Depending on an over coupled (blue), critically coupled (yellow) and under coupled (red) state, the resonator reaches values up to 30000 at room temperature (black circles) and 85000 at cryogenic temperatures (grey diamonds). To study resonators with even higher values an artificial enhancement (feedback-loop) is required.

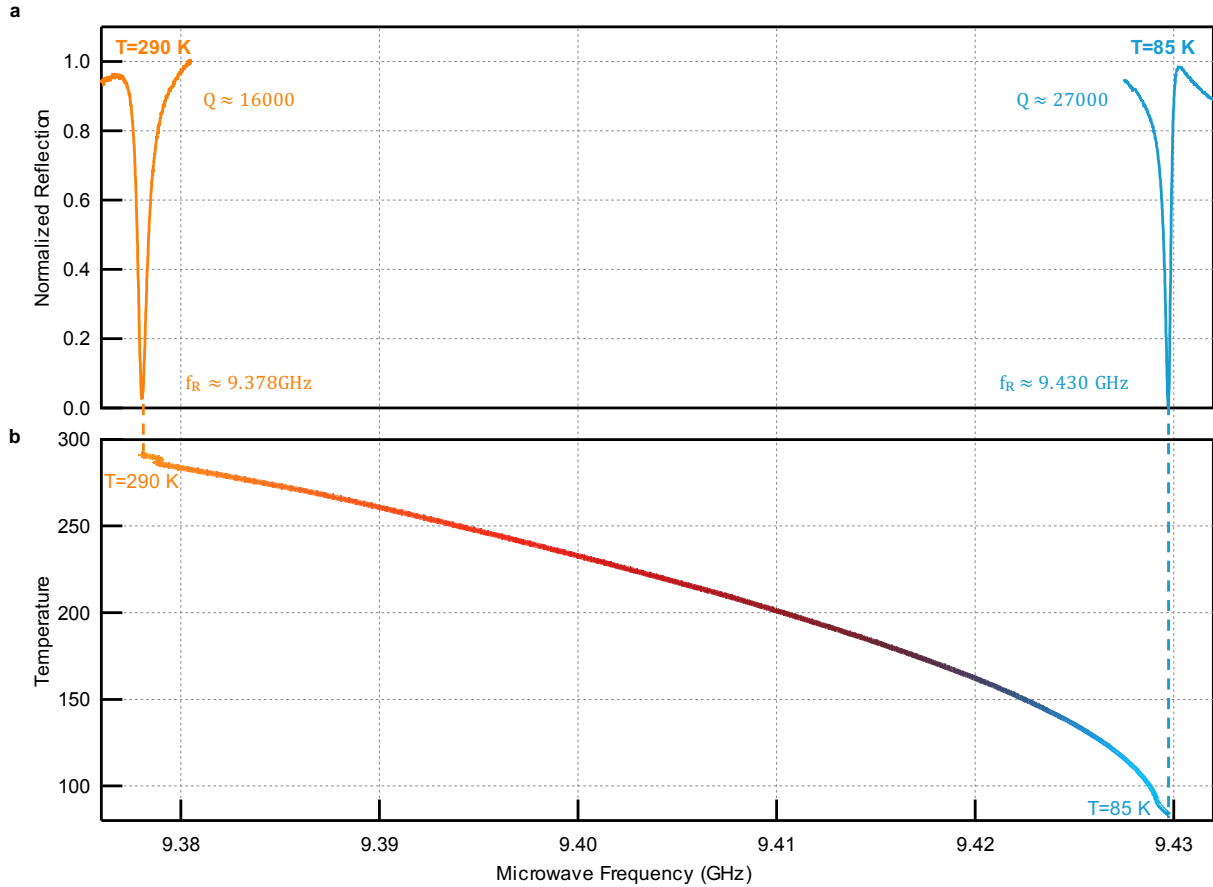


Figure S10. Temperature dependence of the resonator: The resonance frequency is shifting by approximately 50 MHz within a temperature range from 85-290 K due to thermal expansion. The Q-factor is measured at 290 K and 85 K. Between the two resonances, an automatic frequency control locks the resonance frequency of the resonator and provides intermediate frequencies for the whole temperature range.

Maser/Amplifier simulation and experimental data

Simulations according to [Jin et al. 2015] were performed with the following parameter set:

Parameter	Value	Source
γ_{eg}	26 s^{-1}	$T_1^{-1}(T=110 \text{ K})$
N	$2.19 \cdot 10^{13}$	see Figure S11
ω_c	$2\pi \cdot 9.3 \text{ GHz}$	Q-factor measurement
T_2^*	100 ns	estimated value
g	0.5 s^{-1}	see Figure S12
P	1-10000 mW	laser power range
Q	$10^4\text{-}10^6$	FB-loop range

γ_{eg} : The value of 26 s^{-1} is extracted from [Simin et al. 2017] for a temperature of $T=110 \text{ K}$.

N : The number of participating spins is determined by dark EPR. The corresponding measurement is depicted in Figure S11. A piece of the SiC wafer (irradiated with 2 MeV electrons with a fluence of $2 \cdot 10^{17} \text{ cm}^{-2}$) was investigated in a Bruker Magnettech ESR5000 at room temperature (Figure S11 a). We used the left transition (Figure S11 b) and compared the double integral (area of the bottom plot) with the value of a reference sample with a known spin number (BDPA in Figure S11c: $n=3.6 \cdot 10^{17}$). Thus we extracted a spin number of $2.7 \cdot 10^{12}$ for the SiC sample resulting in a spin density of $2.27 \cdot 10^{15} \text{ cm}^{-3}$. The total volume of the sample used for the maser/amplifier/refrigerator is 0.0344 cm^3 resulting in a total spin number of $7.8 \cdot 10^{13}$. The spin number for one transitions (see Figure 1b) is reduced to $\frac{1}{2} \cdot 56.1\% \cdot 7.8 \cdot 10^{13} = 2.19 \cdot 10^{13}$ taking the two transitions (B_+ and B_-) and the isotopic ratio of silicon (see [Gottscholl et al. 2022] for detailed discussion) into account.

ω_c : The value of $2\pi \cdot 9.3 \text{ GHz}$ is based on Q-factor measurements. Small variations can be observed between the measurements, however, the difference is in the MHz regime.

T_2^* : In general, the value is expected in the range of several 100 ns [Carter et al. 2015, Lekavicius et al. 2022]. Here, we choose a typical literature value of about 100 ns since we are dealing with a large ensemble where magnetic field inhomogeneities have a greater impact. An experimental determination is not possible, since the magnetic field inhomogeneity (which limits the T_2^* time) is not comparable between different setups. Pulsed measurements are not realized in the here reported setup due to the long ring-down time of the high-Q resonator. Nevertheless, a precise knowledge of this value is not required, since a small deviation of the actual value leads to only a small shift of the used model parameter g .

g : There is no easy access to the coupling of the microwave photons and the spins. Therefore, we used this parameter as a free parameter to model our whole system. We used the maser measurement with a small output power (result of Figure 1c) as a reference point for the maser threshold, since all other maser measurements provide a much higher maser output. Thus, we varied the coupling g which results in a shift of the maser threshold in Q-factor direction. A few examples are shown in Figure S12. We choose a value of $g = 0.50 \text{ s}^{-1}$ which fits the experimental data quite well.

P : The value of the laser power is swept in the range of 1 mW and 10 W since this is within the experimental achievable range (*K808FANFA-15.00W* laser from *BWT*).

Q : The Q-factor axis was plotted for 10^4 - 10^6 . Values of 10^4 - 10^5 are reached by an under coupling of the resonator (see Figure S9). Values exceeding 10^5 are only possible via a feed-back loop which can be automatically activated and controlled by a microcontroller.

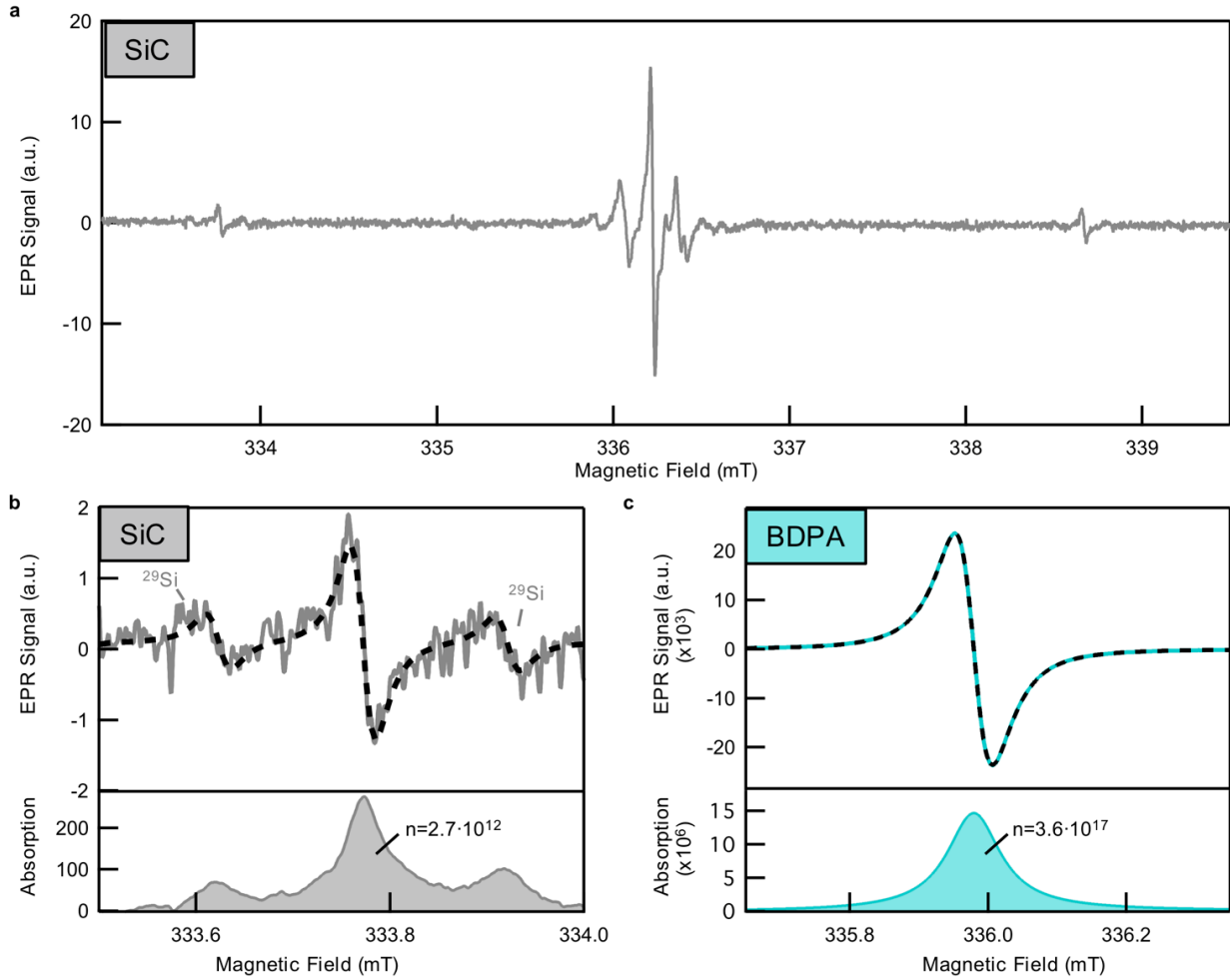


Figure S11: Quantitative EPR measurements for determining the absolute spin number. **a** Room temperature continuous wave EPR measurement without illumination of a SiC sample used in this paper. **b** Zoom into the left transition in order to get only the contribution of the V2 defect. The double integral is proportional to the absolute spin number n . **c** EPR spectrum of a reference sample (BDPA) with known spin number.

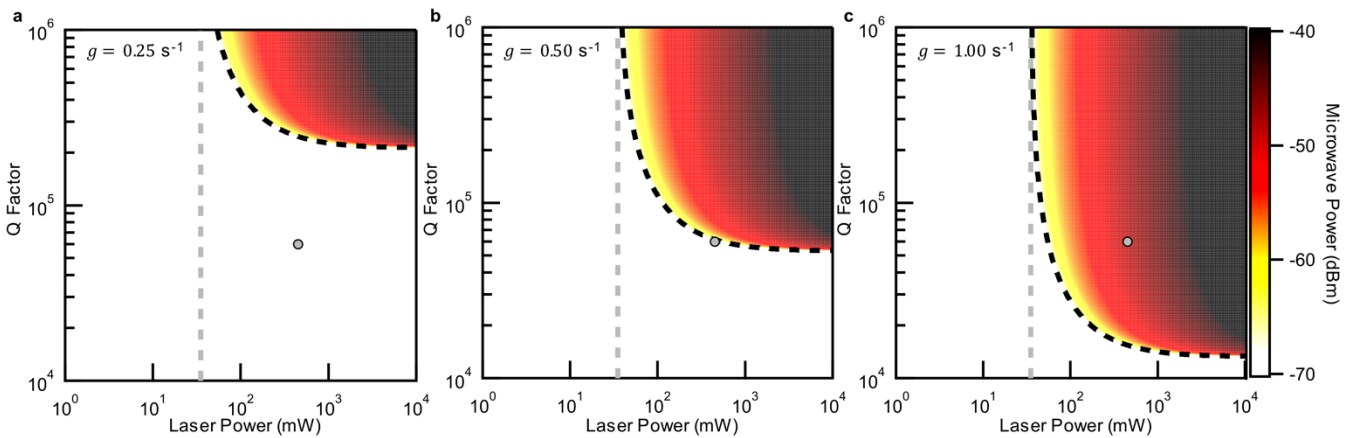


Figure S12. Maser simulations for different couplings g : **a**: $g = 0.25 \text{ s}^{-1}$, **b**: $g = 0.50 \text{ s}^{-1}$ and **c**: $g = 1.00 \text{ s}^{-1}$. The grey circle illustrates the maser measurement of Figure 1c. Since the output power is very small, we expect the maser threshold to be in this parameter range. Thus, we can adjust the unknown value of the coupling accordingly.

Further measurements and simulations

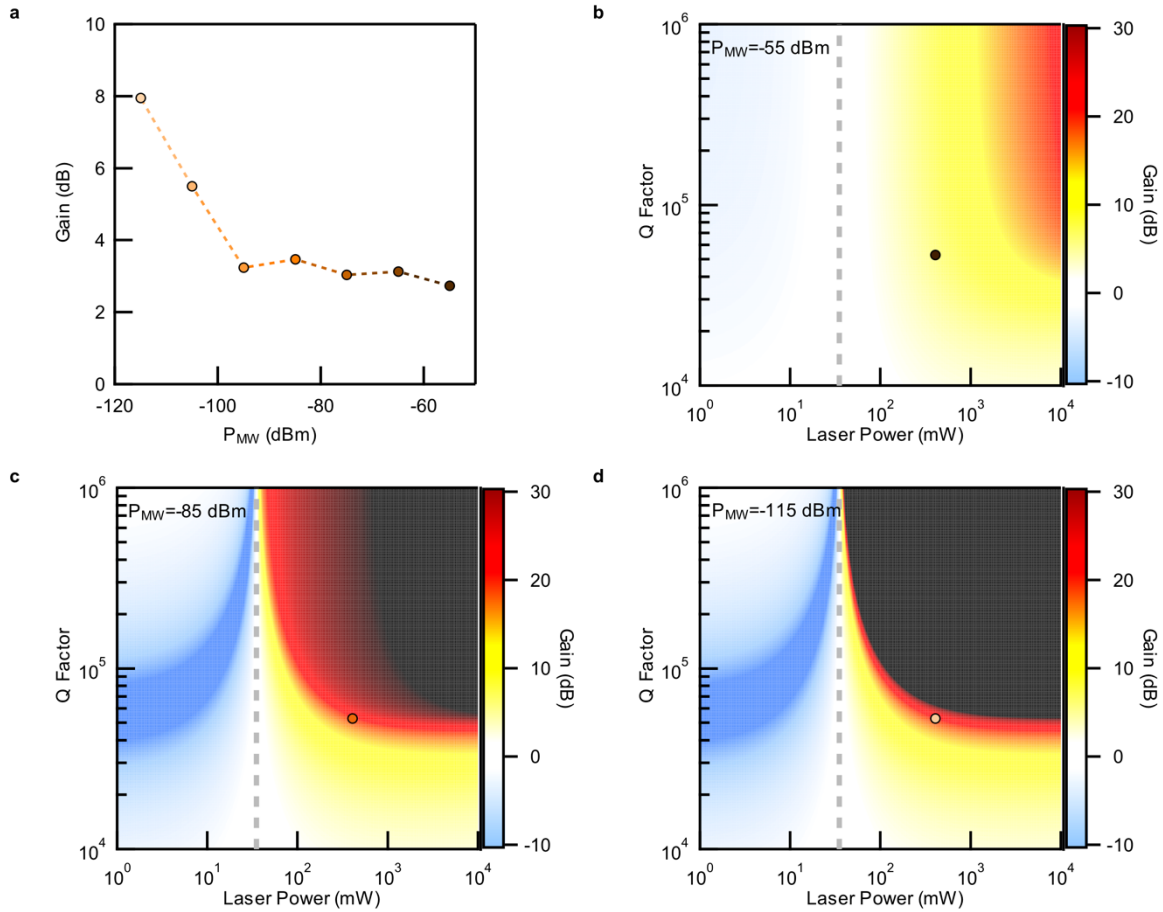


Figure S13. Power dependent SiC-based amplifier: **a** Measured gain for various input powers. **b-d** Simulations for different microwave input powers (-55dBm, -85dBm, -115dBm). A higher gain is expected for smaller incoming signals, which fits qualitatively to the experimental observation.

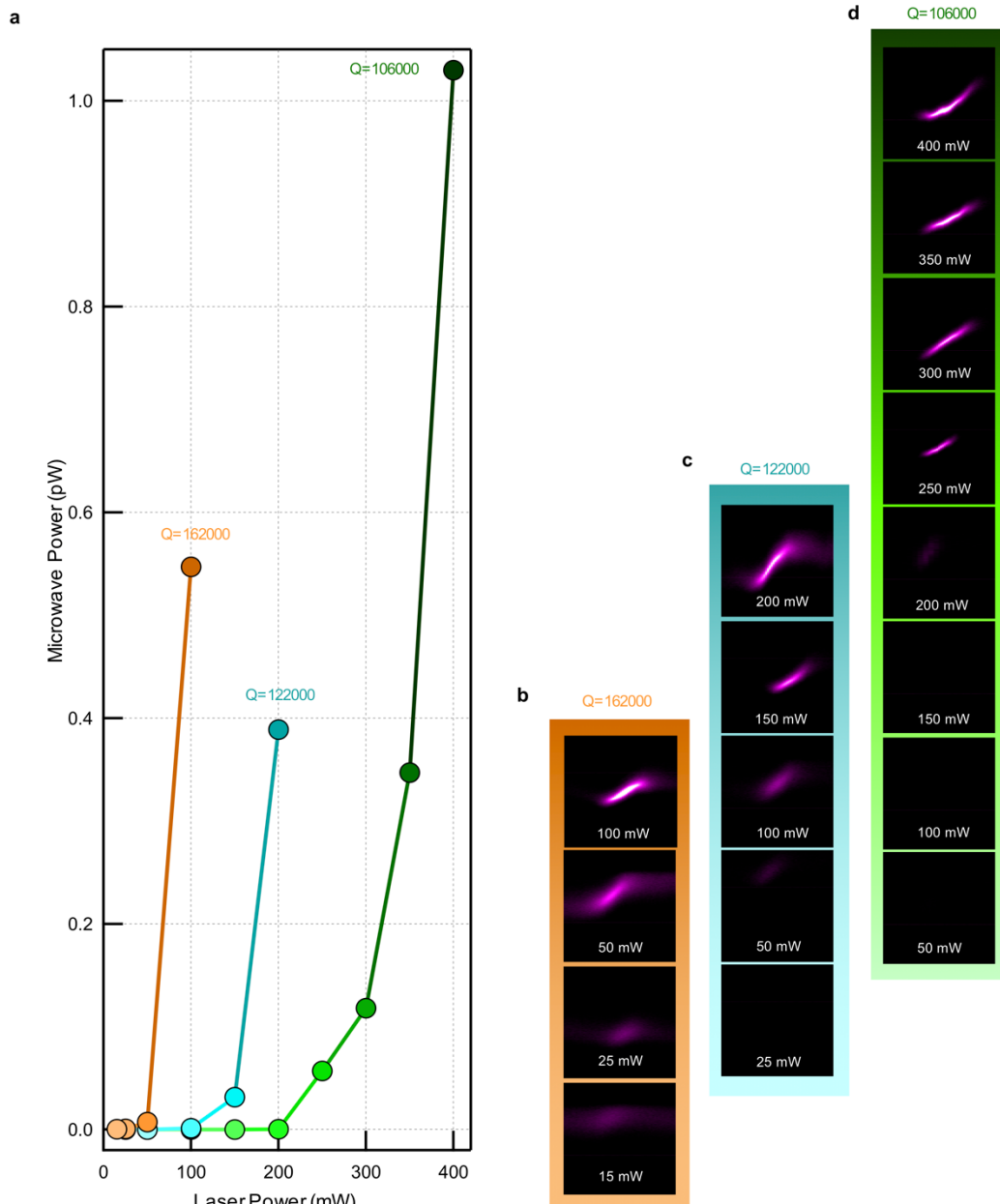


Figure S14. Overview of Q-boosted maser measurements for different laser power and Q-factors: This figure summarizes the data sets which were used in the main text in Figure 2c. **a** Extracted microwave power for different Q-factors and pump powers. **b** Maser measurements for Q-factors of 162000 (orange), **c** 122000 (blue) and **d** 106000 (green). The color maps represent the microwave output power (pink) analog to Figure 2b in the main text. As expected from the simulations, masing occurs for higher Q-factors at lower pump powers.

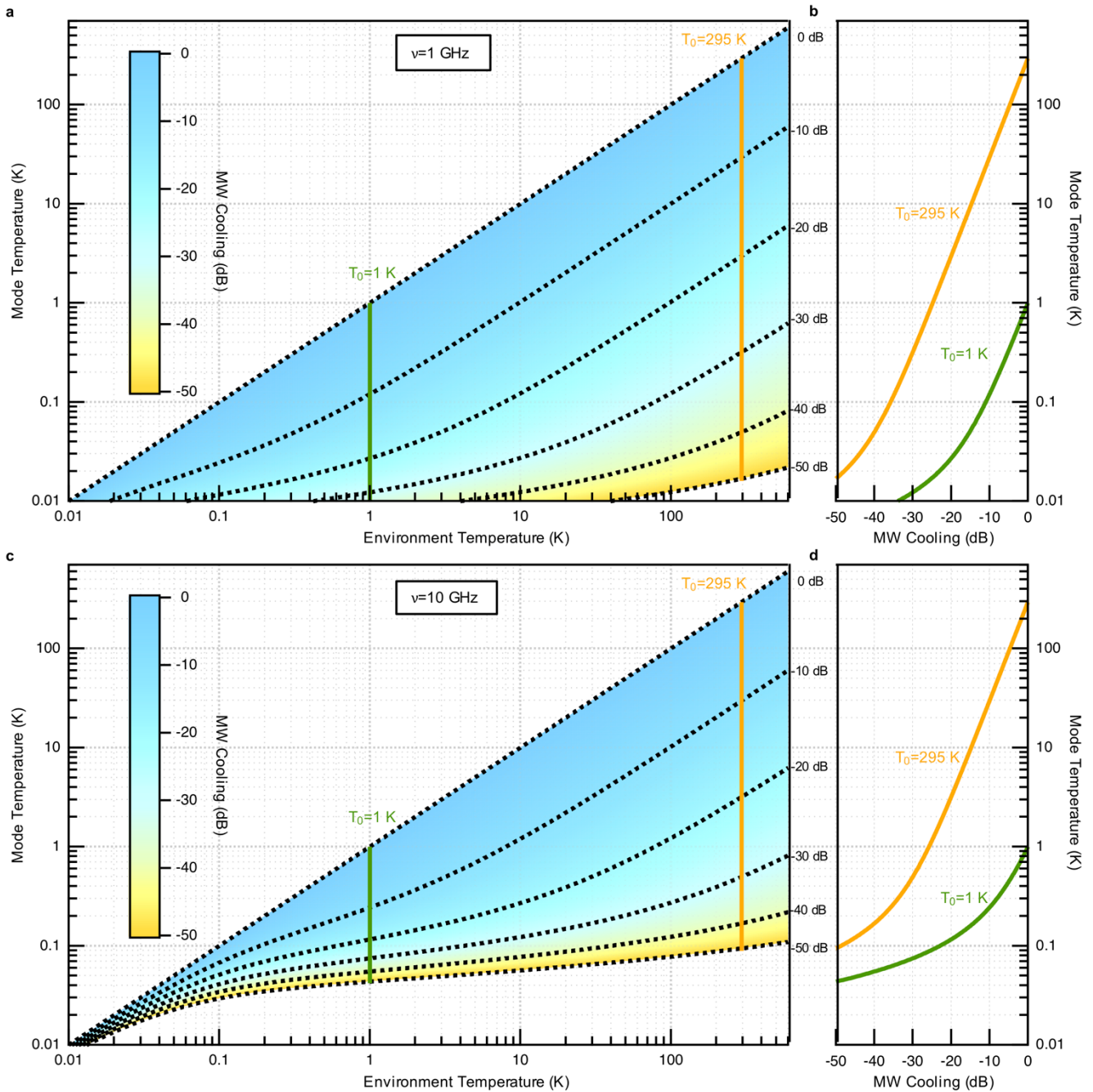


Figure S15. Simulation of the required microwave cooling to achieve a specific mode temperature for various environment temperatures: **a** The color map reveals the potential for a device operating a 1 GHz. To address the applicability, we inserted two cross sections at 1 K (as a reference value for superconducting qubits) and 295 K (for room temperature application) displayed in green and orange, respectively. **b** Reveals the required cooling to reach a specific mode temperature. **c** and **d** display the same simulations for a 10 GHz system.

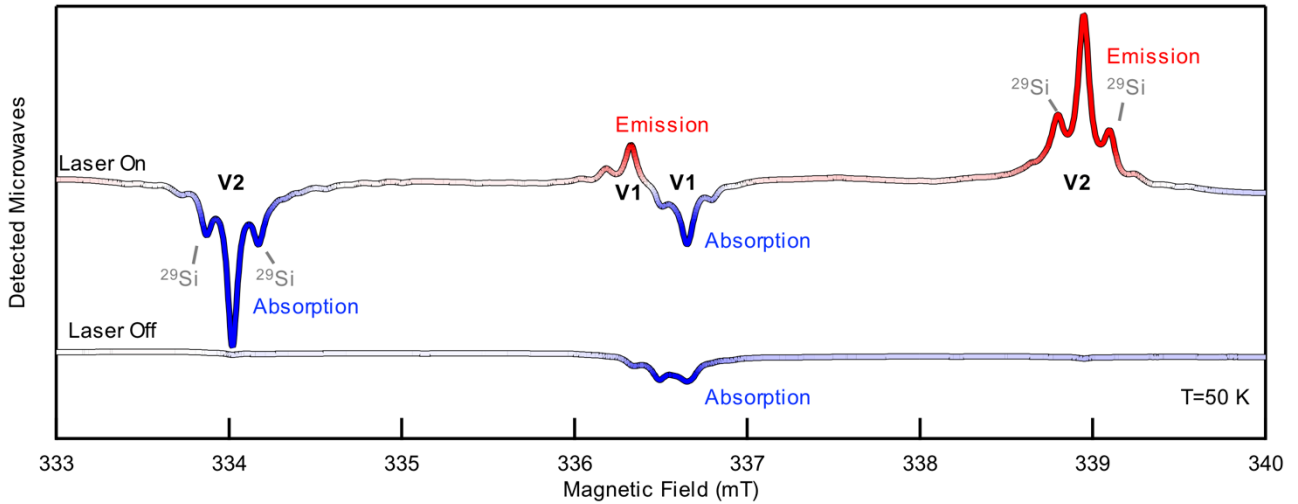


Figure S16. Comparison of the silicon vacancies V1 and V2: The detected microwaves (integrated EPR signal) under illumination reveal the absorptive and emissive character of both defects at different magnetic fields. For proof-of-concept measurements, the V2 is favored since the effect of emission and absorption is larger and therefore easier to test for an amplifier/refrigerator. For future application of a magnetic switching of amplifier and microwave cooling devices (e.g. quantum computing) we recommend the V1 defect, since the field difference of the absorptive and emission transition is in the range of $\Delta B \approx 325 \mu\text{T}$ due to the smaller ZFS.